Percorso Didattico Scientifico Specializzazione Radio-Oncologia

GLIOMI DI ALTO GRADO

Giulia Butera

31-01-2020

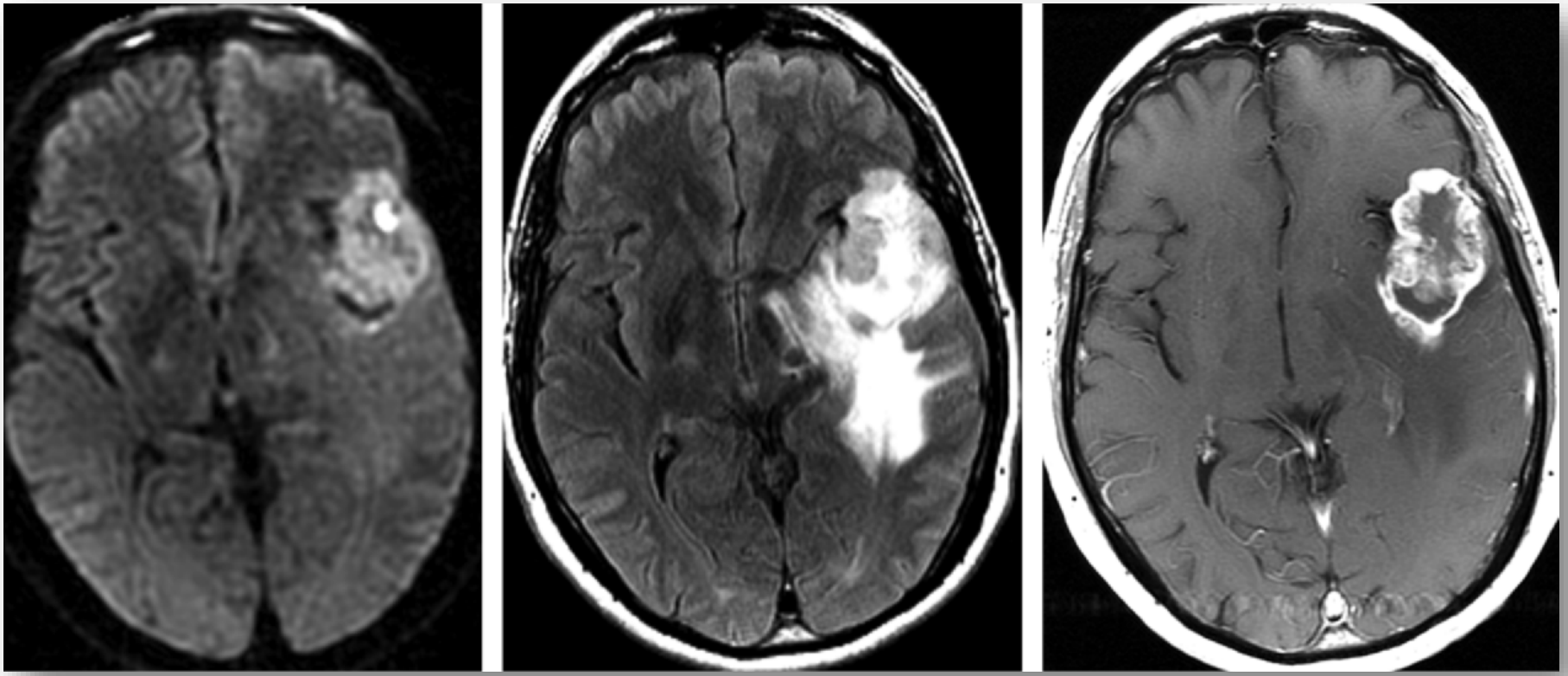

GLIOBLASTOMA

Caratterizzare:

- Aggressività
- Risposta alla terapia
- Sopravvivenza

CELLULARITA'
VASCOLARIZZAZIONE
CARATTERISTICHE MOLECOLARI

CELLULARITA' E AGGRESSIVITA'

•Il **movimento random** delle molecole di H_2O può essere misurato tramite l'applicazione di gradienti che rendano la sequenza (Spin Echo T_2) sensibile alla diffusione.

•Il gradiente è una disomogeneità lineare nel campo magnetico e quindi nel volume in esame che a sua volta crea disomogeneità nella frequenza di precessione degli spin (marca gli spin magneticamente).

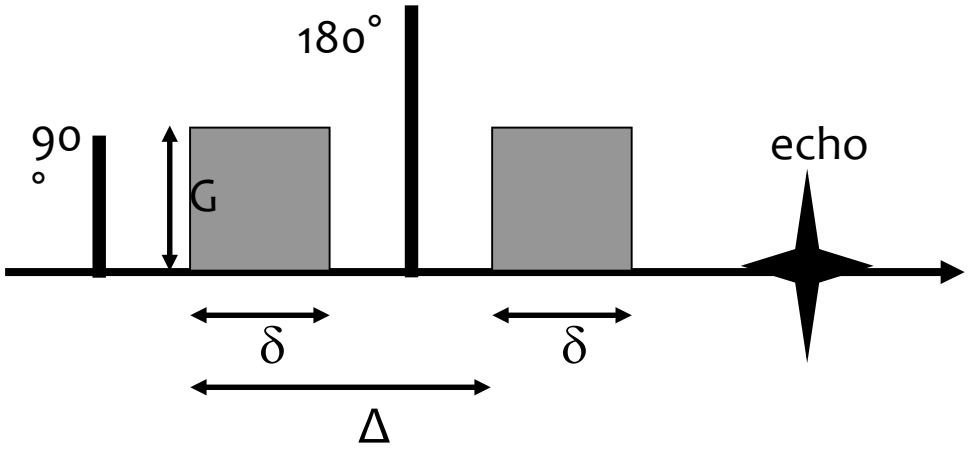

Diffusione: Stejskal-Tanner

Il peso in diffusione b determina una diminuzione dell'ampiezza dell'eco; la caduta del segnale è proporzionale al coefficiente di diffusione D delle molecole.

Perchè siamo interessati a misurare la diffusione (D) nei tessuti biologici?

La microstruttura del tessuto stesso determina la mobilità delle particelle influenzandone il moto casuale....

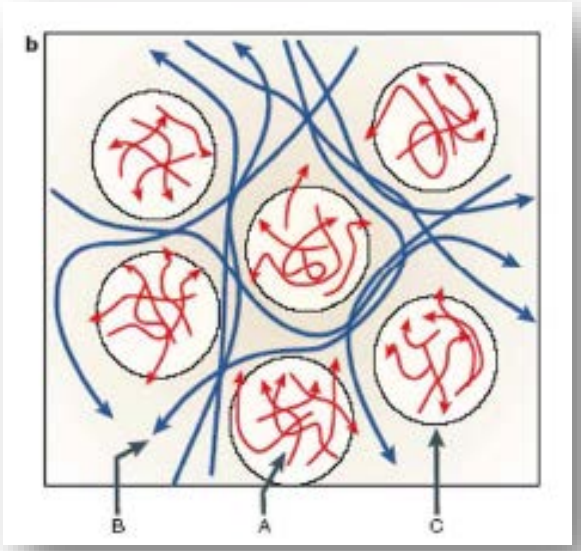

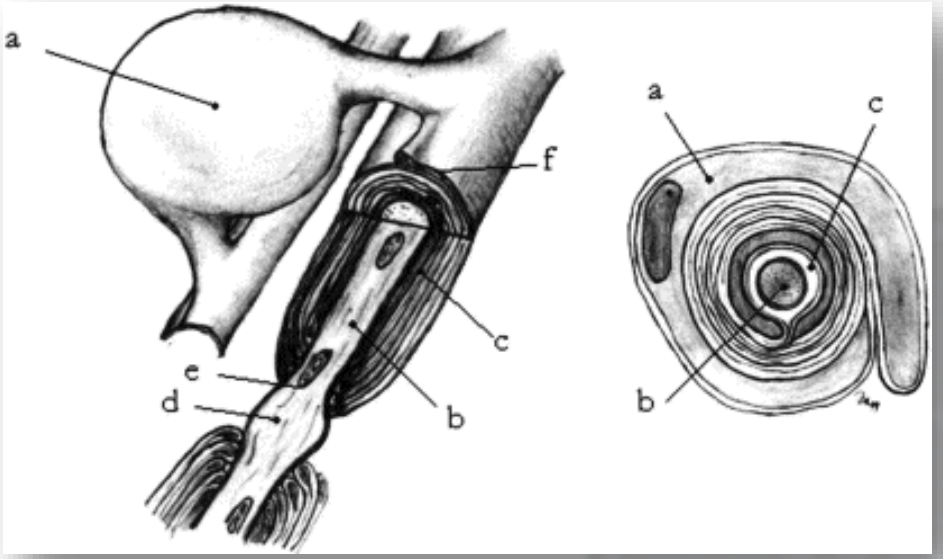

Conosco **D** ⟶ conosco la **microstruttura**

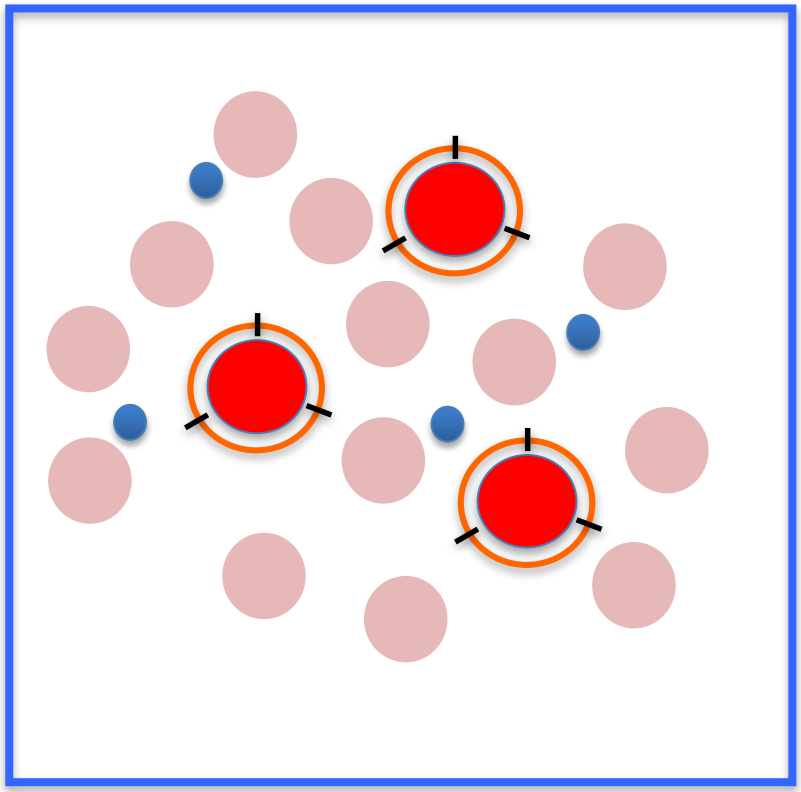

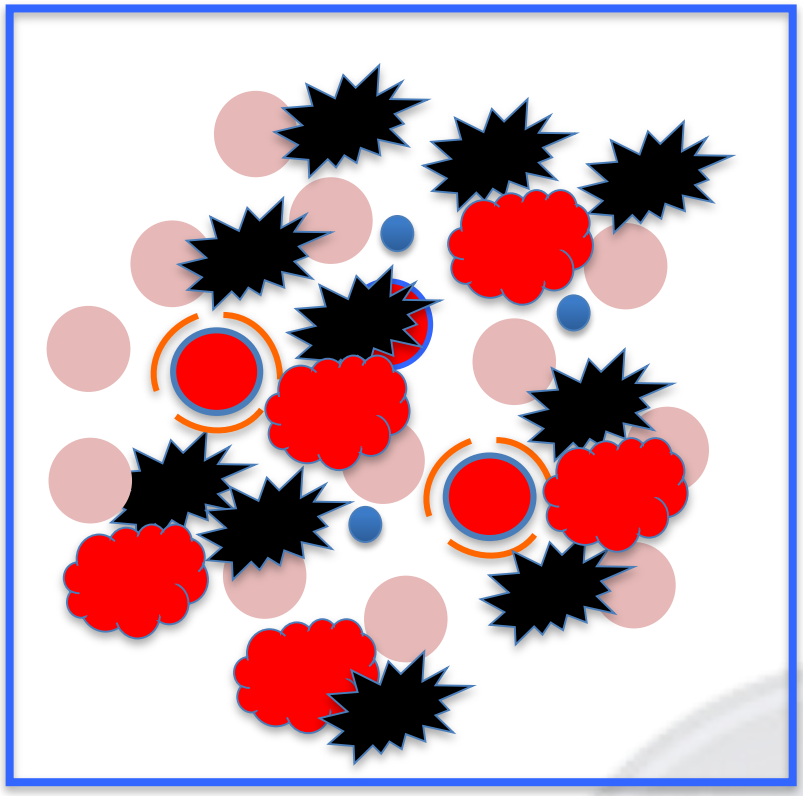

RIDOTTA DIFFUSIVITA' DELLE MOLECOLE D'ACQUA

AUMENTO DEL SEGNALE IN DWI
RIDOTTI VALORI DI ADC

DIFFUSIONE ED ADC

- la diffusività delle neoplasie cerebrali è in genere aumentata (elevato segnale ADC)
- una diffusività ristretta (basso ADC) può essere presente in alcuni tumori nella componente solida
- tipicamente sono tumori con elevata cellularità (PNET, linfomi, metastasi)

J Magn Reson Imaging. 1999 Jan;9(1):53-60.

Usefulness of diffusion-weighted MRI with echo-planar technique in the evaluation of cellularity in gliomas.

Sugahara T, Korogi Y, Kochi M, Ikushima I, Shigematu Y, Hirai T, Okuda T, Liang L, Ge Y, Komohara Y, Ushio Y, Takahashi M.

Department of Radiology, Kumamoto University School of Medicine, Japan. sugatake@kaiju.medic.kumamoto-u.ac.jp

Radiology. 2005 Jun;235(3):985-91. Epub 2005 Apr 15.

Apparent diffusion coefficient of human brain tumors at MR imaging.

Yamasaki F, Kurisu K, Satoh K, Arita K, Sugiyama K, Ohtaki M, Takaba J, Tominaga A, Hanaya R, Yoshioka H, Hama S, Ito Y, Kajiwara Y, Yahara K, Saito T, Thohar MA.

Dept of Neurosurgery, Graduate School of Biomedical Sciences, Hiroshima Univ, 1-2-3 Kasumi, Minami-ku, Hiroshima 734-8551, Japan.

AJNR Am J Neuroradiol. 2001 Jun-Jul;22(6):1081-8.

The role of diffusion-weighted imaging in patients with brain tumors.

Kono K, Inoue Y, Nakayama K, Shakudo M, Morino M, Ohata K, Wakasa K, Yamada R.

Department of Radiology, Izumi Municipal Hospital, Izumi-shi , Osaka, Japan.

...esiste una correlazione indiretta tra cellularità e ADC min nei gliomi (P = 0.007)...

Nel contesto del tumore le regioni con basso valore di ADC min rappresentano i siti di spiccata angiogenesi ed elevata densità cellulare come descritto da ***Barajas et al (Radiology 2010)***


[AH]
[PF]

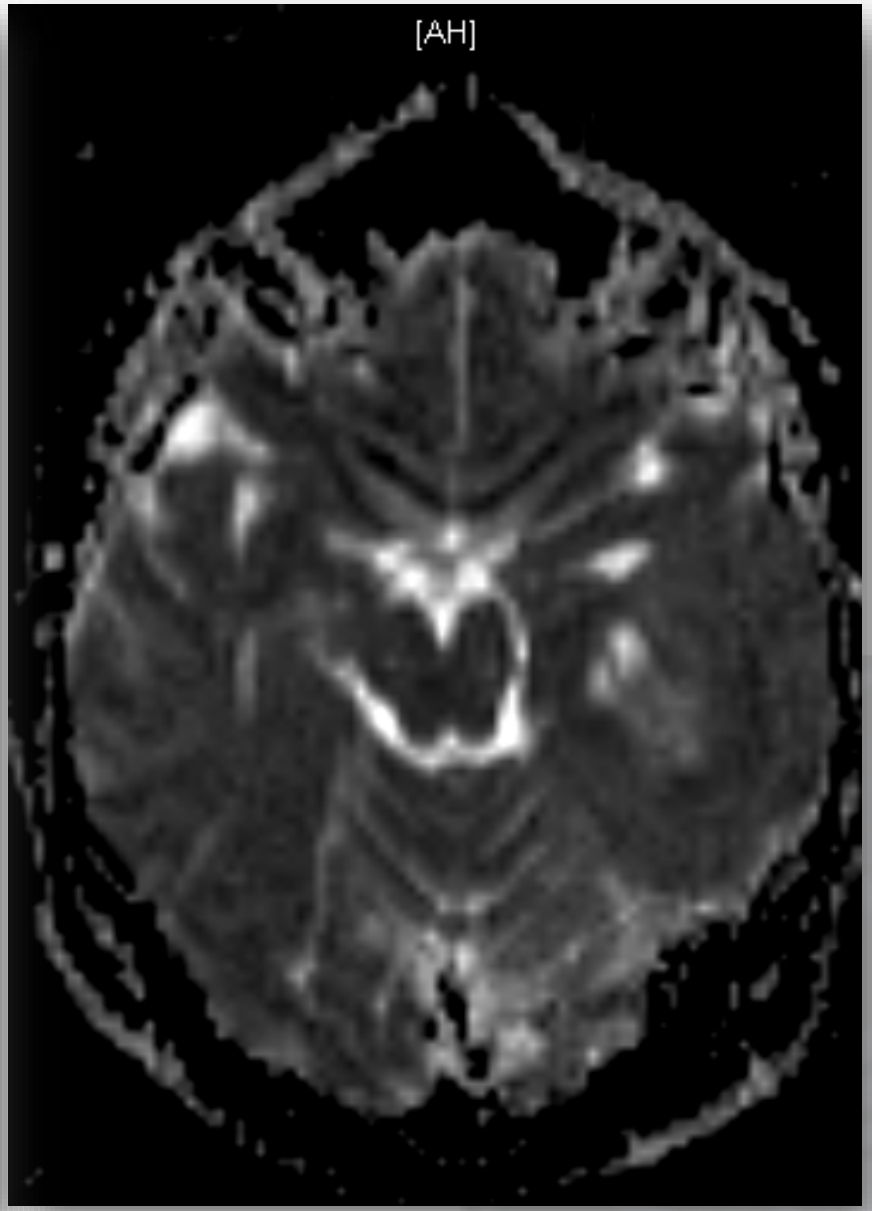
[AH]

VASCOLARIZZAZIONE & AGGRESSIVITA'

PARAMETRI EMODINAMICI: POTENZIAMENTO

- il potenziamento è espressione di danno della BEE
- ad eccezione dell'atrocitoma pilocitico è espressione di grading avanzato
- la presenza di aree ipovascolarizzate può essere dovuta a cisti o aree di necrosi
- la regolarità della parete è tipica delle cisti; viceversa per la necrosi

A causa della presenza della barriera emato-encefalica, i mezzi di contrasto attualmente a disposizione non possono raggiungere il tessuto cerebrale

Ostacolo al passaggio di sostanza lipofobiche nel cervello

Passaggio consentito solo a sostanza liposolubili (ossigeno, etanolo, ormoni steroidei) o tramite sistemi “carrier” (zucchero, aminoacidi)

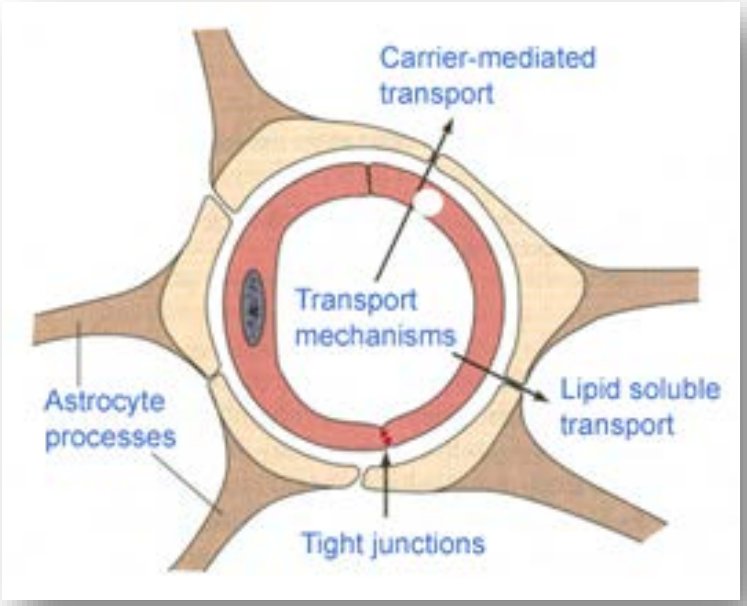

In presenza di tumori cerebrali, in particolare gliomi, la BEE può subire danni per la presenza di NEO-ANGIOGENESI e per DANNO DIRETTO DEL TUMORE

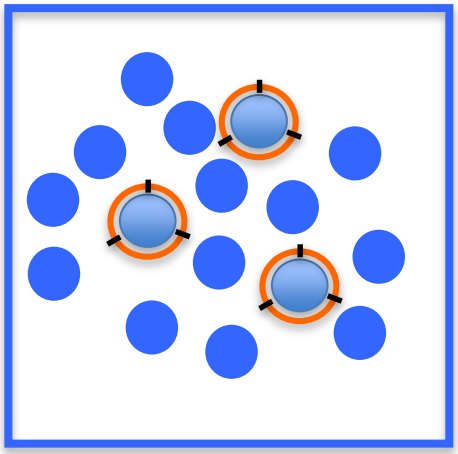

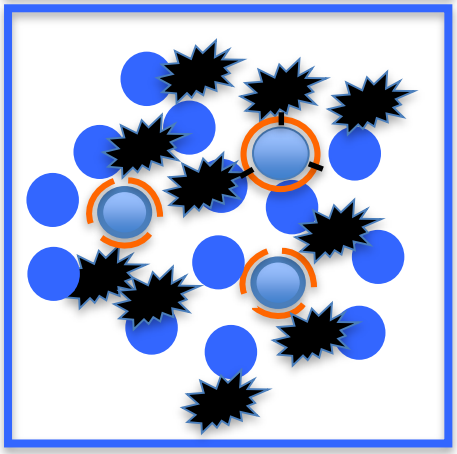

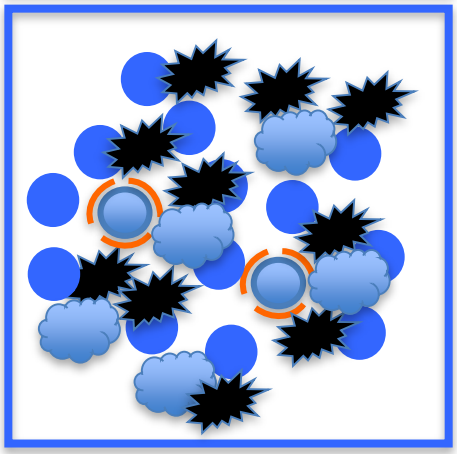

Durante la crescita del glioma e nelle fasi di viraggio a più alto grado di malignità, non esiste una adeguato apporto ematico allaumentata richiesta metabolica dovuta alla rapida proliferazione neoplastica.

L'ipossia generatasi porta ad una stimolazione del **fattore di crescita endoteliale vasoattivo** e lo sviluppo di una nuova vascolarizzazione chiamata angiogenesi.

La neo-vascolarizzazione è sprovvista di BEE, alterata anche dalla crescita del tumore stesso, fenomeno che porta ad una aumentata permeabilità endoteliale.

PERFUSIONE

Dinamic Susceptibility Contrast Imaging

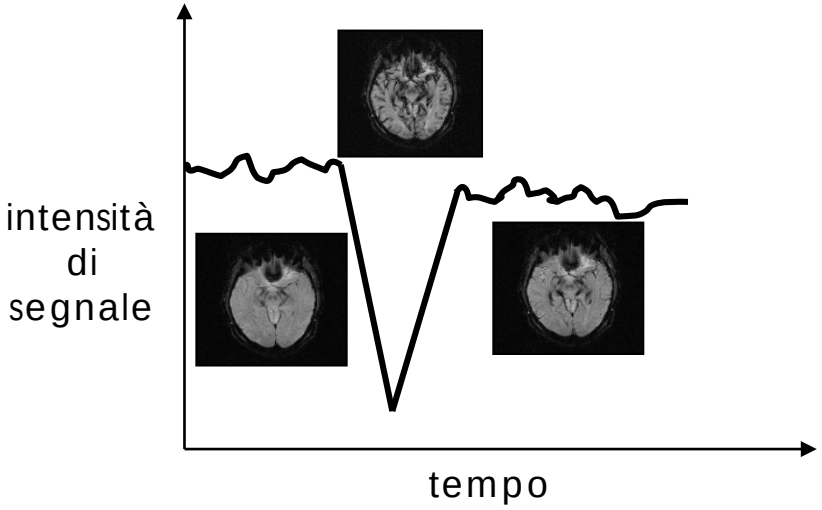

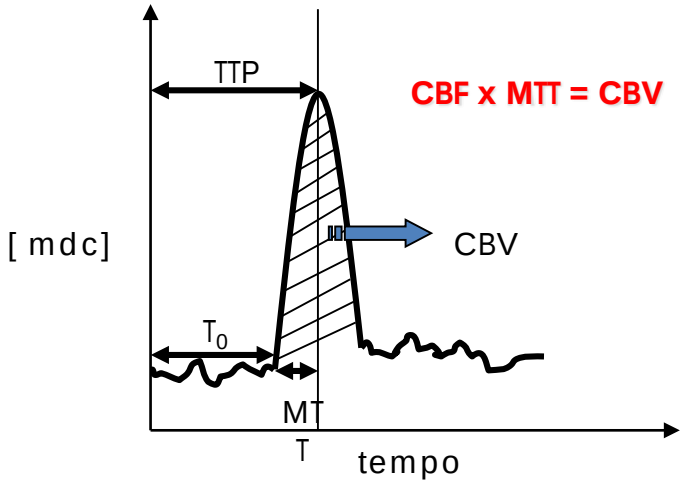

iniettare un mezzo di contrasto a bolo e di osservarne il passaggio attraverso l'encefalo

Valutazione della NEOANGIOGENESI tumorale mediante rCBV

GRADING tumorale terapia

rCBV: indice di sopravvivenza

Indici di PERMEABITA'

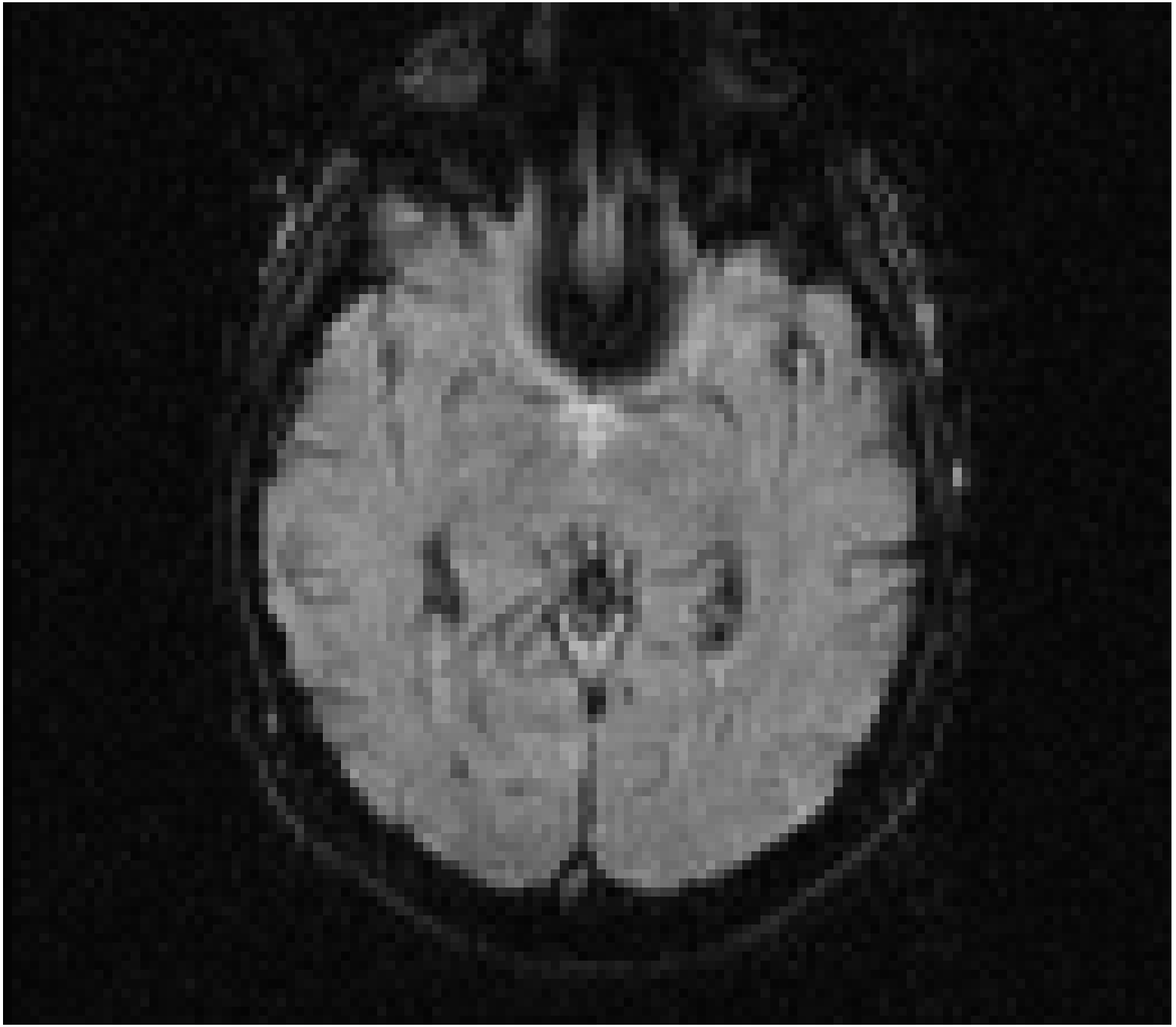

AJNR Am J Neuroradiol 24:1989–1998, November/December 2003

Glioma Grading: Sensitivity, Specificity, and Predictive Values of Perfusion MR Imaging and Proton MR Spectroscopic Imaging Compared with Conventional MR Imaging

Meng Law, Stanley Yang, Hao Wang, James S. Babb, Glyn Johnson, Soonmee Cha, Edmond A. Knopp, and David Zagzag

RM convenzionale: 55-83% di sensibilità
rCBV: 95% sensibilità, 57% specificità usando 1.75 come valore soglia

AJNR Am J Neuroradiol 26:777–783, April 2005

MR Cerebral Blood Volume Maps Correlated with Vascular Endothelial Growth Factor Expression and Tumor Grade in Nonenhancing Gliomas

Antonio C. M. Maia, Jr, Suzana M. F. Malheiros, Antonio J. da Rocha, Carlos J. da Silva, Alberto A. Gabbai, Fernando A. P. Ferraz, and João N. Stávale

Esiste una correlazione tra i valori di rCBV e l'espressione di VEGF

Low-Grade Gliomas: Dynamic Susceptibility-weighted Contrast-enhanced Perfusion MR Imaging—Prediction of Patient Clinical Response[1]

Radiology

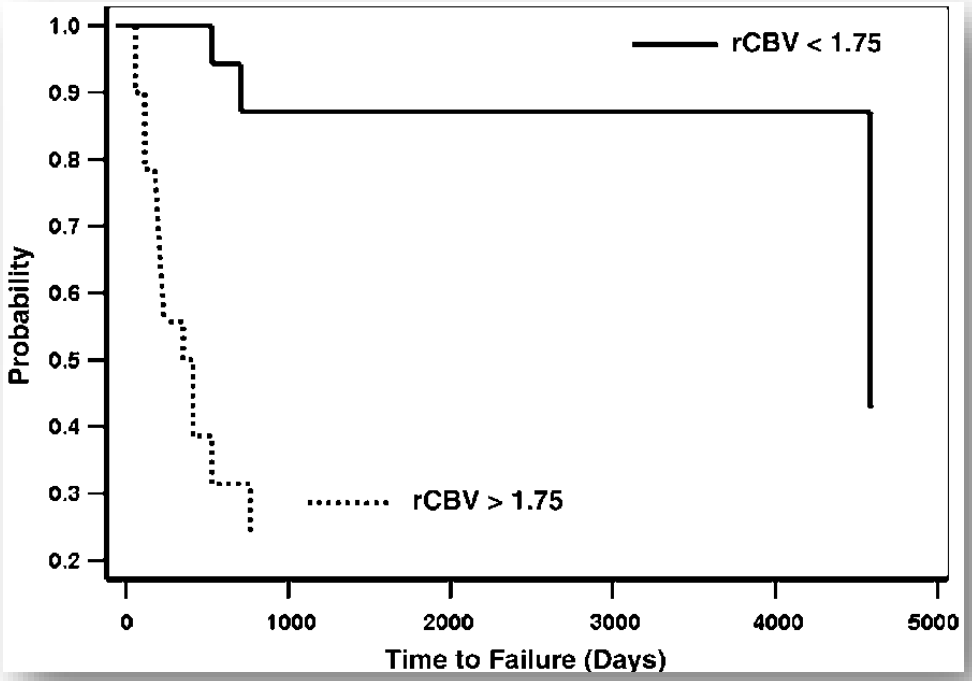

Lesioni con rCBV minore di 1.75 hanno un tempo medio di progressione di 4620 giorni (DS 433), quelle con valore maggiore di 1.75 un tempo medio di progressione di 245 (DS 62).

Journal of Neuro-Oncology (2018) 139:455–460
https://doi.org/10.1007/s11060-018-2887-4

CLINICAL STUDY

Prediction of survival in patients affected by glioblastoma: histogram analysis of perfusion MRI

Andrea Romano[1] · Luca Pasquini[2] · Alberto Di Napoli[2] · Francesca Tavanti[2] · Alessandro Boellis[2] · Maria Camilla Rossi Espagnet[2,4] · Giuseppe Minniti[3,5] · Alessandro Bozzao[2]

Received: 30 December 2017 / Accepted: 8 April 2018 / Published online: 2 May 2018

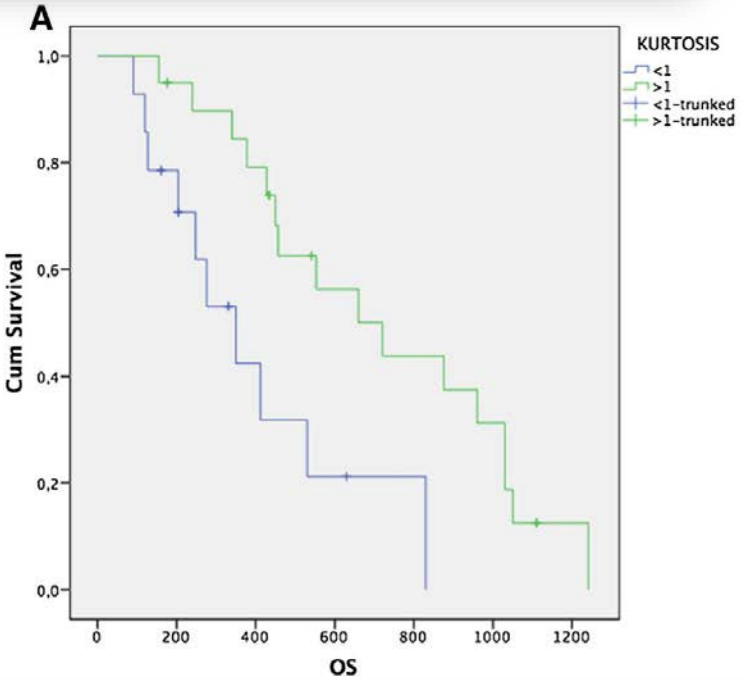

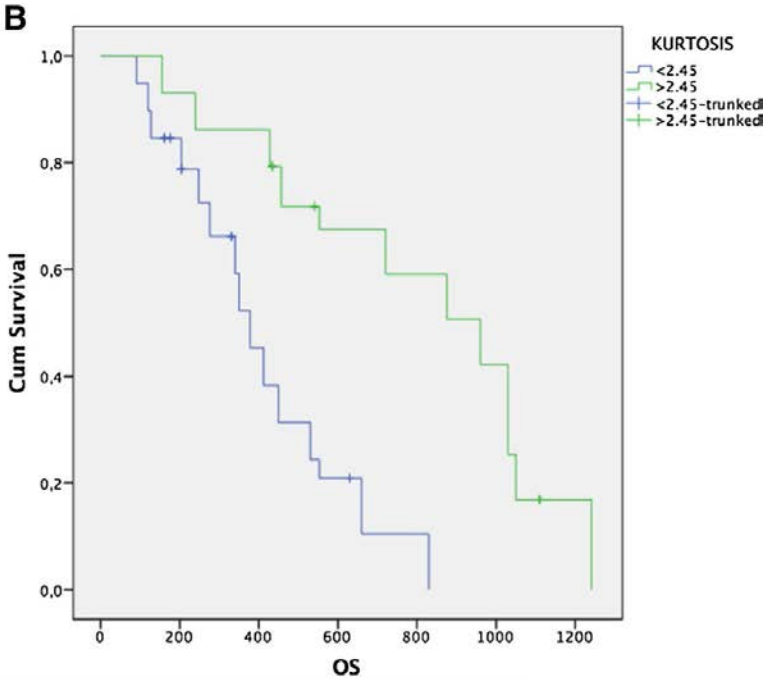

RESULTS: rCBV kurtosis and rCBV skewness showed significant differences between subjects surviving > 1 and > 2 years, According to ROC analysis, the rCBV kurtosis showed the best statistic performance compared to the other parameters; respectively, values of 1 and 2.45 represented an optimised cut-off point to distinguish subjects surviving over 1 or 2 years. Kaplan-Meier curves showed a significant difference between subjects with rCBV kurtosis values higher or lower than 1 (respectively 1021 and 576 days; Log-rank test: p = 0.007), and between subjects with rCBV kurtosis values higher or lower than 2.45 (respectively 802 and 408 days; Log-rank test: p = 0.001).

CONCLUSION: The histogram analysis of perfusion MRI proved to be a valid method to predict survival in patients affected by glioblastoma.

BIOLOGIA MOLECOLARE

Acta Neuropathol (2016) 131:803–820
DOI 10.1007/s00401-016-1545-1

REVIEW

The 2016 World Health Organization Classification of Tumors of the Central Nervous System: a summary

David N. Louis[1] · Arie Perry[2] · Guido Reifenberger[3,4] · Andreas von Deimling[4,5] · Dominique Figarella-Branger[6] · Webster K. Cavenee[7] · Hiroko Ohgaki[8] · Otmar D. Wiestler[9] · Paul Kleihues[10] · David W. Ellison[11]

Diffuse astrocytic and oligodendroglial tumours	
Diffuse astrocytoma, IDH-mutant	9400/3
Gemistocytic astrocytoma, IDH-mutant	9411/3
Diffuse astrocytoma, IDH-wildtype	*9400/3*
Diffuse astrocytoma, NOS	9400/3
Anaplastic astrocytoma, IDH-mutant	9401/3
Anaplastic astrocytoma, IDH-wildtype	*9401/3*
Anaplastic astrocytoma, NOS	9401/3
Glioblastoma, IDH-wildtype	9440/3
Giant cell glioblastoma	9441/3
Gliosarcoma	9442/3
Epithelioid glioblastoma	*9440/3*
Glioblastoma, IDH-mutant	9445/3*
Glioblastoma, NOS	9440/3
Diffuse midline glioma, H3 K27M–mutant	9385/3*
Oligodendroglioma, IDH-mutant and 1p/19q-codeleted	9450/3
Oligodendroglioma, NOS	9450/3
Anaplastic oligodendroglioma, IDH-mutant and 1p/19q-codeleted	9451/3
Anaplastic oligodendroglioma, NOS	*9451/3*
Oligoastrocytoma, NOS	*9382/3*
Anaplastic oligoastrocytoma, NOS	*9382/3*

WHO grades of select CNS tumours	
Diffuse astrocytic and oligodendroglial tumours	
Diffuse astrocytoma, IDH-mutant	II
Anaplastic astrocytoma, IDH-mutant	III
Glioblastoma, IDH-wildtype	IV
Glioblastoma, IDH-mutant	IV
Diffuse midline glioma, H3 K27M–mutant	IV
Oligodendroglioma, IDH-mutant and 1p/19q-codeleted	II
Anaplastic oligodendroglioma, IDH-mutant and 1p/19q-codeleted	III
Other astrocytic tumours	
Pilocytic astrocytoma	I
Subependymal giant cell astrocytoma	I
Pleomorphic xanthoastrocytoma	II
Anaplastic pleomorphic xanthoastrocytoma	III

GLIOMI ALTO GRADO

NEUROLOGIC AND EMERGENCY IMAGING 1717

RadioGraphics

Genetics of Glioblastoma: A Window into Its Imaging and Histopathologic Variability[1]

TEACHING POINTS See last page

Clifford J. Belden, MD • Pablo A. Valdes, PhD • Cong Ran, BS • David A. Pastel, MD • Brent T. Harris, MD, PhD • Camilo E. Fadul, MD • Mark A. Israel, MD • Keith Paulsen, PhD • David W. Roberts, MD

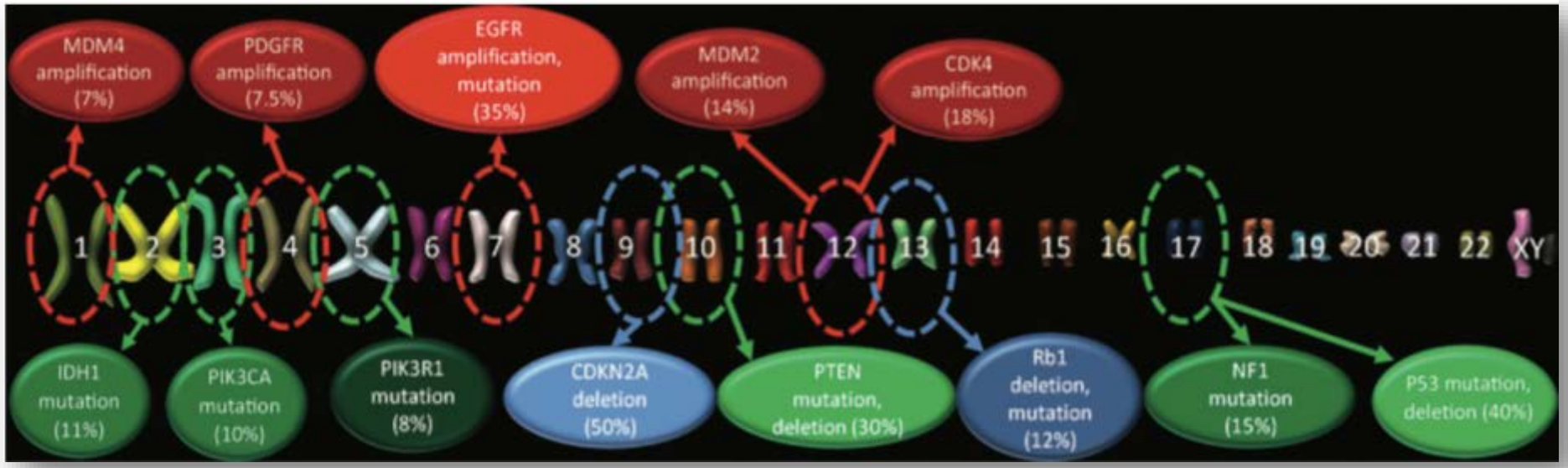

Common Genetic Alterations in Glioblastomas

The common genetic alterations that occur in glioblastomas have been catalogued in recent studies by using data from the Cancer Genome Atlas Research Network; a typical glioblastoma harbors more than 60 genetic alterations (2–4). Nearly 90% of these alterations are mutations (including deletions), and the remaining 10% are chromosomal aberrations (amplifications) (Fig 1)

understood. For radiologists, understanding the common genetic alterations (mutations, amplifications, and deletions), changes in gene expression, and resulting tumor biology are important for the following reasons: *(a)* imaging features of glioblastomas may correlate with gene expression, *(b)* imaging may provide a noninvasive technique to assess both spatial and temporal changes in gene expression, and *(c)* understanding the molecular and cellular changes that occur in glioblastomas is helpful in interpreting imaging findings in patients undergoing molecular-targeted therapies.

GLIOMI ALTO GRADO:

RadioGraphics
NEUROLOGIC AND EMERGENCY IMAGING 1717

Genetics of Glioblastoma: A Window into Its Imaging and Histopathologic Variability[1]

TEACHING POINTS See last page

Clifford J. Belden, MD • Pablo A. Valdes, PhD • Cong Ran, BS • David A. Pastel, MD • Brent T. Harris, MD, PhD • Camilo E. Fadul, MD • Mark A. Israel, MD • Keith Paulsen, PhD • David W. Roberts, MD

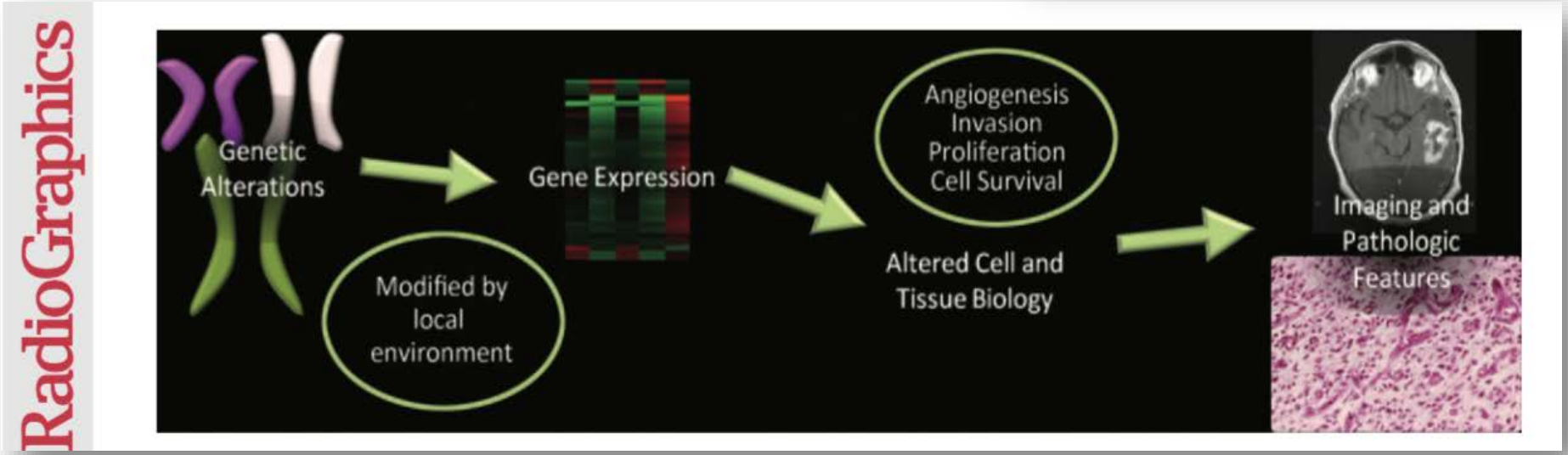

Effects of Genetic Changes on Gene Expression and Tumor Biology

The effects of genetic alterations in glioblastoma are further enhanced by local factors such as pH level, hypoxia, hormones, growth factors, and other epigenetic factors, and they lead to changes in expression of the altered genes. As a result, both spatial and temporal variations in gene expression occur, which ultimately manifest in the tumor biology and are reflected in the heterogeneous imaging features and pathologic findings of glioblastoma. The changes in angiogenesis, cellular proliferation, cellular invasion, and cell survival and apoptosis that occur in patients with glioblastoma correlate with distinct imaging and pathologic features (Fig 5).

SIGNIFICATIVA CORRELAZIONE TRA PARAMETRI MOLECOLARI E PROGNOSI

- *MUTAZIONE IDH*
- *VEGF*
- *EGFR*
- *STATO DI METILAZIONE DEL PARAMETRO MGMT*

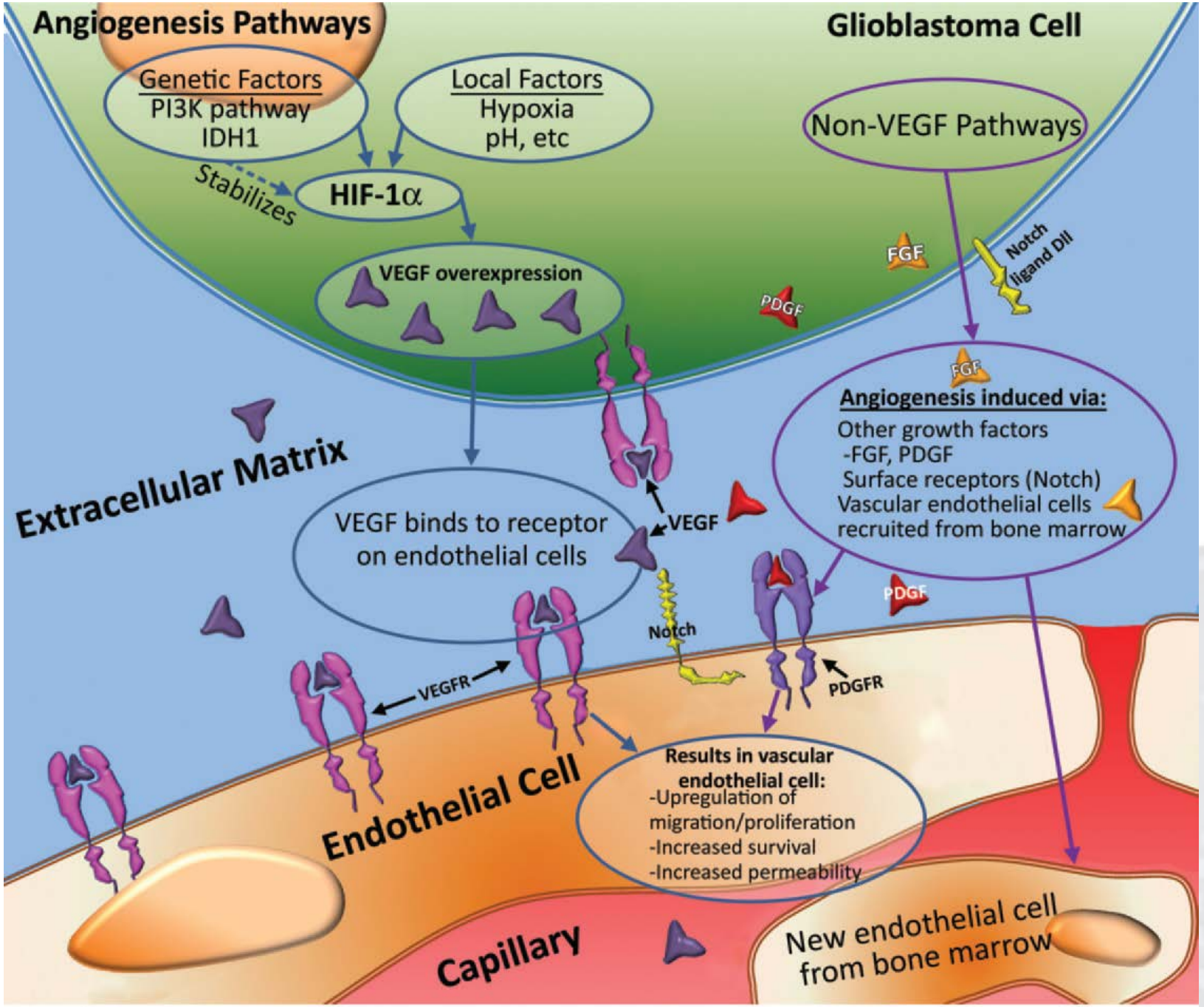
Angiogenesis Pathways
Glioblastoma Cell
Genetic Factors
PI3K pathway
IDH1
Local Factors
Hypoxia
pH, etc
Non-VEGF Pathways
Stabilizes
HIF-1α
VEGF overexpression
FGF
Notch ligand Dll
PDGF
FGF
Angiogenesis induced via:
Other growth factors
-FGF, PDGF
Surface receptors (Notch)
Vascular endothelial cells recruited from bone marrow
Extracellular Matrix
VEGF binds to receptor on endothelial cells
VEGF
PDGF
Notch
VEGFR
PDGFR
Endothelial Cell
Results in vascular endothelial cell:
-Upregulation of migration/proliferation
-Increased survival
-Increased permeability
Capillary
New endothelial cell from bone marrow

Mutazione isocitrato deidrogenasi IDH1/2

ASPETTO PROSPETTICO DELL'EVOLUZIONE NEOPLASTICA E PROGNOSI

70% dei gliomi di II-III grado

80% dei glioblastomi secondari

10% dei glioblastomi primitivi

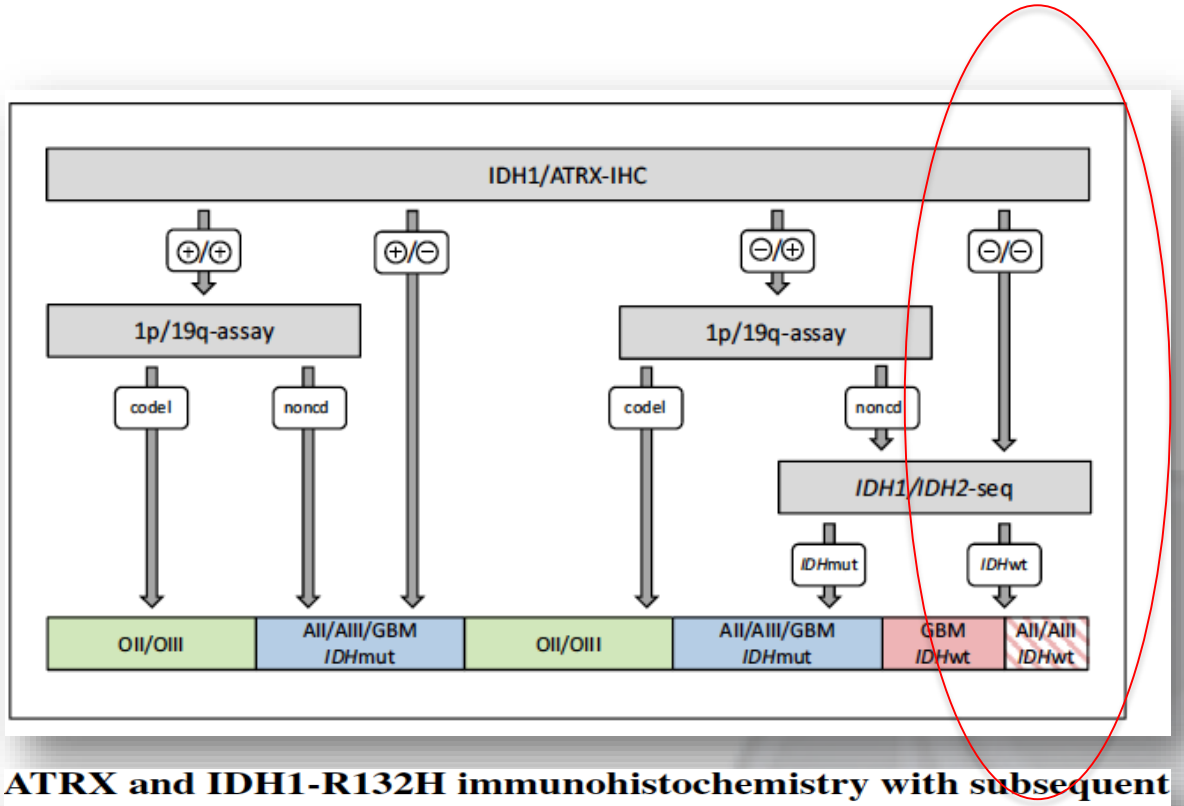

ATRX and IDH1-R132H immunohistochemistry with subsequent copy number analysis and *IDH* sequencing as a basis for an "integrated" diagnostic approach for adult astrocytoma, oligodendroglioma and glioblastoma

David E. Reuss · Felix Sahm · Daniel Schrimpf · Benedikt Wiestler · David Capper · Christian Koelsche · Leonille Schweizer · Andrey Korshunov · David T. W. Jones · Volker Hovestadt · Michel Mittelbronn · Jens Schittenhelm · Christel Herold-Mende · Andreas Unterberg · Michael Platten · Michael Weller · Wolfgang Wick · Stefan M. Pfister · Andreas von Deimling

Acta Neuropathol (2015) 129:133–146

ADC vs IDH1/2

sensibilità (50%)
specificità (91%)

J Neurooncol (2015) 121:141–150
DOI 10.1007/s11060-014-1614-z

CLINICAL STUDY

Evaluation of the microenvironmental heterogeneity in high-grade gliomas with *IDH1/2* gene mutation using histogram analysis of diffusion-weighted imaging and dynamic-susceptibility contrast perfusion imaging

Seunghyun Lee · Seung Hong Choi · Inseon Ryoo · Tae Jin Yoon · Tae Min Kim · Se-Hoon Lee · Chul-Kee Park · Ji-Hoon Kim · Chul-Ho Sohn · Sung-Hye Park · Il Han Kim

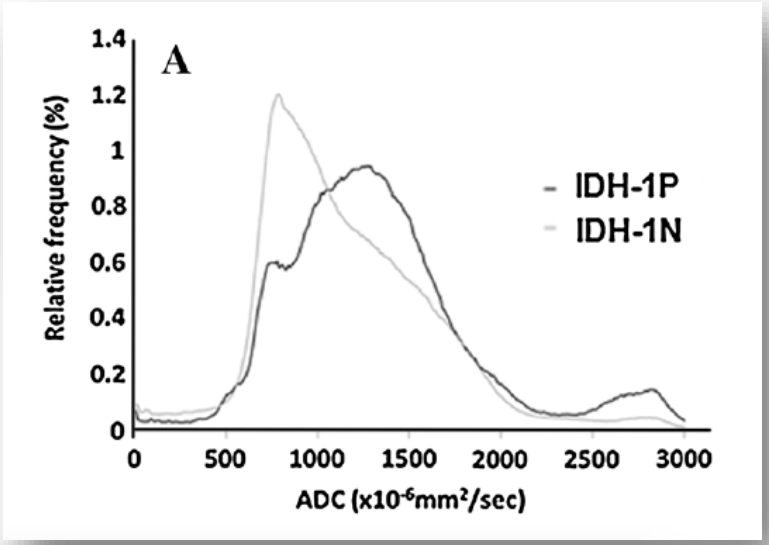

The mean ADC value was higher in the *IDH1* ^{P} group than *IDH1* ^{N} (1,282.8 vs. 1,159.6 mm^2/s, *P* = .0113).

ADC : 1,333x10^{-6}mm^2/sec

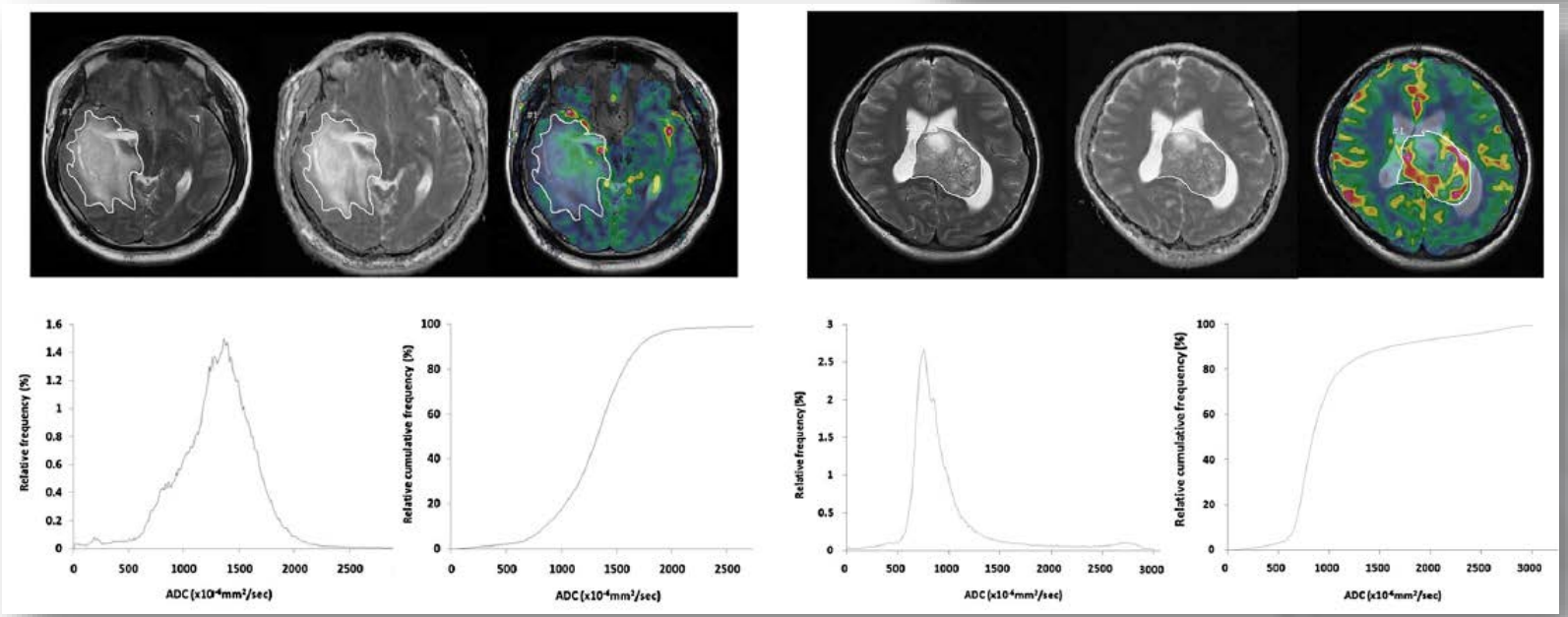

IDH genotypes differentiation in glioblastomas using DWI and DSC-PWI in the enhancing and peri-enhancing region

Acta Radiologica
0(0) 1–10

DOI: 10.1177/0284185119842288
journals.sagepub.com/home/acr
SAGE

Zhen Xing*, Hua Zhang*, Dejun She, Yu Lin, Xiaofang Zhou, Zheng Zeng and Dairong Cao

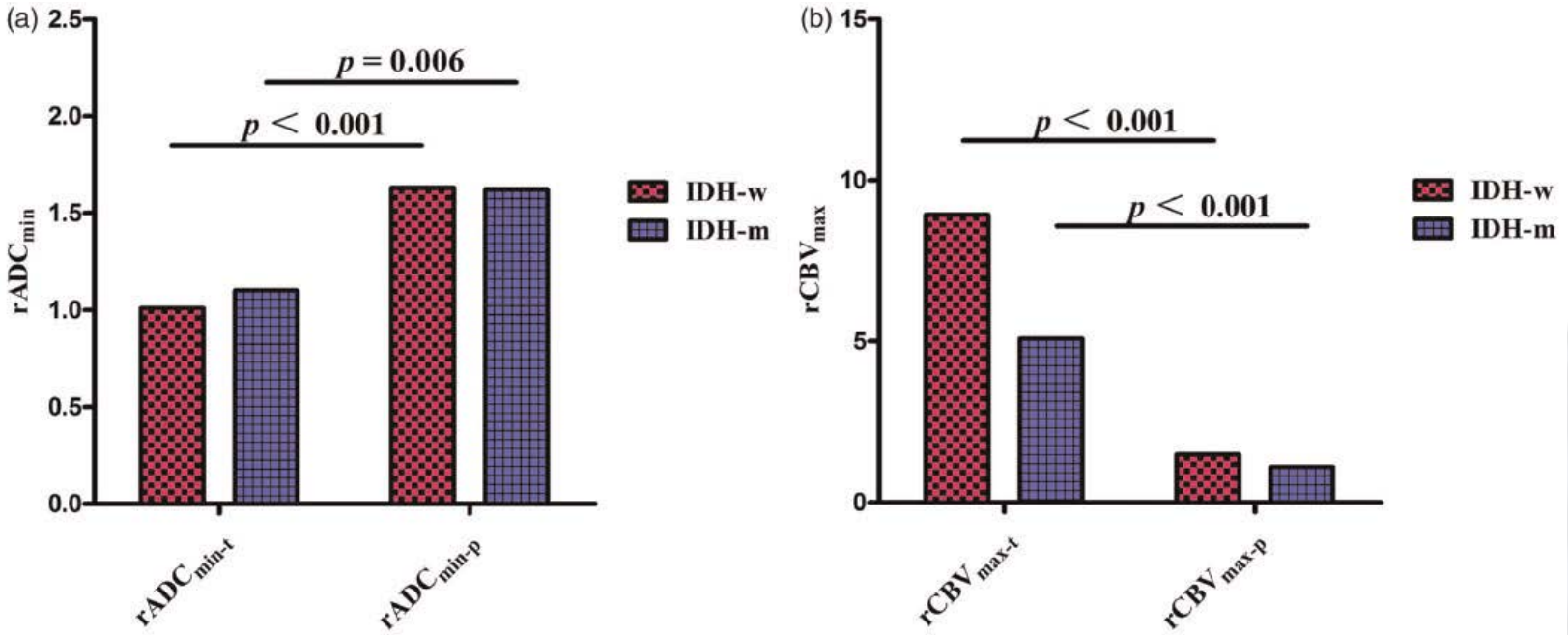

RESULTS IDH-m glioblastomas tended to present in frontal lobes and younger patients. The rADC$_{min-t}$ (P = 0.042) were significantly lower in IDH-w than IDH-m. Both rCBV$_{max-t}$ and rCBV$_{max-p}$ showed significant differences between two subgroups (all P < 0.001). The optimal cutoff values in prediction of IDH-m were >0.98 for rADC$_{min-t}$, <7.27 for rCBV$_{max-t}$, and < 0.97 for rCBV$_{max-p}$. Multivariate logistic regression revealed that the combination of rADC$_{min-t}$ and rCBV$_{max-t}$ yielded the highest sensitivity and specificity.

CONCLUSION: The rCBV$_{max-t}$ or rCBV$_{max-p}$ may serve as preferable and comparable imaging biomarkers for evaluation of glioblastomas IDH status. The combination of rADC$_{min-t}$ and rCBV$_{max-t}$ may yield the maximum predictive power for differentiating IDH status.

Radiology

Nicoletta Anzalone, MD
Antonella Castellano, MD, PhD
Marcello Cadioli, MSc
Gian Marco Conte, MD
Valeria Cuccarini, MD
Alberto Bizzi, MD
Marco Grimaldi, MD
Antonella Costa, MD
Giovanni Grillea, MD
Paolo Vitali, MD, PhD
Domenico Aquino, MSc
Maria Rosa Terreni, MD
Valter Torri, MD
Bradley J. Erickson, MD, PhD
Massimo Caulo, MD, PhD

Brain Gliomas: Multicenter Standardized Assessment of Dynamic Contrast-enhanced and Dynamic Susceptibility Contrast MR Images[1]

ORIGINAL RESEARCH ■ NEURORADIOLOGY

Purpose: To evaluate the feasibility of a standardized protocol for acquisition and analysis of dynamic contrast material–enhanced (DCE) and dynamic susceptibility contrast (DSC) magnetic resonance (MR) imaging in a multicenter clinical setting and to verify its accuracy in predicting glioma grade according to the new World Health Organization 2016 classification.

Comparison and Parameter	A_z value	Confidence Interval*	*P* Value	Cutoff Value	Sensitivity (%)	Specificity (%)
Lower-grade glioma (WHO II or III) vs glioblastoma (WHO IV)†						
v_p	0.847	0.769, 0.925	<.0001	3.06	85.7	70.8
K^{trans}	0.831	0.741, 0.921	<.0001	0.045	85.7	76.5
v_e	0.853	0.772, 0.934	<.0001	16.23	85.7	78.4
iAUC	0.842	0.760, 0.924	<.0001	0.122	85.7	74.5
rCBV	0.894	0.830, 0.958	<.0001	6.71	85.7	80.4
WHO II vs WHO III/IV glioma						
v_p	0.868	0.796, 0.939	<.0001	1.50	86.4	71.4
K^{trans}	0.903	0.841, 0.965	<.0001	0.015	86.4	85.7
v_e	0.903	0.838, 0.967	<.0001	1.75	87.9	85.7
iAUC	0.906	0.846, 0.965	<.0001	0.049	86.4	82.1
rCBV	0.898	0.833, 0.963	<.0001	3.33	86.4	85.7

Table 2

Hotspot Values of v_p, K^{trans}, v_e, iAUC, and rCBV for Different Tumor Grades

Parameter	WHO II (n = 28)	WHO III (n = 23)	WHO IV Glioblastoma (n = 43)	*P* Value* II vs III†	II vs IV†	III vs IV†	II/III vs IV‡
v_p (mL/100 g)	0.805 (0.532–1.477)	3.247 (0.849–6.484)	6.707 (5.458–8.695)	.019 (.017)	<.0001 (<.0001)	.023 (.009)	<.0001 (<.0001)
K^{trans} (min^{-1})	0.004 (0.001–0.008)	0.040 (0.009–0.113)	0.079 (0.063–0.106)	.004 (.001)	<.0001 (<.0001)	.068 (.068)	<.0001 (<.0001)
v_e (%)	0.0 (0.0–0.0)	14.5 (0.0–28.4)	27.3 (20.22–35.58)	.004 (.002)	<.0001 (<.0001)	.027 (.016)	<.0001 (<.0001)
iAUC	0.02 (0.010–0.028)	0.13 (0.038–0.205)	0.20 (0.162–0.227)	.004 (.001)	<.0001 (<.0001)	.050 (.040)	<.0001 (<.0001)
rCBV	2.05 (1.534–2.516)	5.70 (2.411–8.825)	11.65 (8.873–13.42)	.019 (.019)	<.0001 (<.0001)	.004 (.001)	<.0001 (<.0001)

Note.—Unless otherwise indicated, data are interpatie
cerebral blood volume, v_e = fractional volume of the e
* $P < .05$ indicates a significant difference between
† Calculated by using Kruskal-Wallis and Dunn tests f
‡ Calculated by using Mann-Whitney *U* test.

Hotspot Values of v_p, K^{trans}, v_e, iAUC, and rCBV for Different Lower-Grade Glioma Molecular Subtypes

Parameter	IDH Mutation and 1p19q Codeletion (n = 13)	IDH Mutation but no 1p19q Codeletion (n = 14)	IDH Mutation (n = 27)	IDH Wild-Type (n = 9)	*P* Value* IDH Mutation and 1p19q Codeletion vs Noncodeletion	IDH Mutation vs IDH Wild-Type
v_p (mL/100 g)	0.921 (0.222–2.944)	1.135 (0.369–5.247)	1.09 (0.532–1.829)	2.91 (0.363–7.461)	>.05	>.05
K^{trans} (min^{-1})	0.008 (0.003–0.280)	0.007 (0.001–0.118)	0.008 (0.003–0.012)	0.009 (0.004–0.091)	>.05	>.05
v_e (%)	0.0 (0.0–18.18)	0.0 (0.0–23.01)	0.0 (0.0–3.59)	0.0 (0.0–14.71)	>.05	>.05
iAUC	0.028 (0.009–0.073)	0.024 (0.002–0.173)	0.025 (0.011–0.063)	0.047 (0.017–0.168)	>.05	>.05
rCBV	1.99 (1.397–5.705)	1.83 (0.944–3.679)	1.98 (1.426–3.667)	2.53 (2.174–9.325)	.056	>.05

Note.—Data are interpatient median values, with ranges in parentheses. iAUC = initial area under the concentration curve, IDH = isocitrate dehydrogenase, K^{trans} = volume transfer constant, rCBV = relative cerebral blood volume, v_e = fractional volume of the extravascular-extracellular space, v_p = fractional volume of the intravascular compartment.

* $P < .05$ indicates a significant difference between groups. *P* values were calculated by using the Mann-Whitney *U* test.

Clinical Radiology 70 (2015) 1087–1095

Contents lists available at ScienceDirect

Clinical Radiology

journal homepage: www.clinicalradiologyonline.net

Pro-angiogenic cellular and genomic expression patterns within glioblastoma influences dynamic susceptibility weighted perfusion MRI

R.F. Barajas Jr.[a], J.J. Phillips[c,d], S.R. Vandenberg[e], M.W. McDermott[c], M.S. Berger[c], W.P. Dillon[b], S. Cha[b,c,*]

Four angiogenic pathways (vascular endothelial growth factor [VEGF], hypoxia inducible factor [HIF], platelet-derived growth factor [PDGF], fibroblast growth factor [FGF]) were significantly up-regulated within enhancing regions when compared to non-enhancing regions.

A statistically significant correlation was observed between VEGF-A expression, microvascular density, microvascular morphology and DSC perfusion MRI metrics

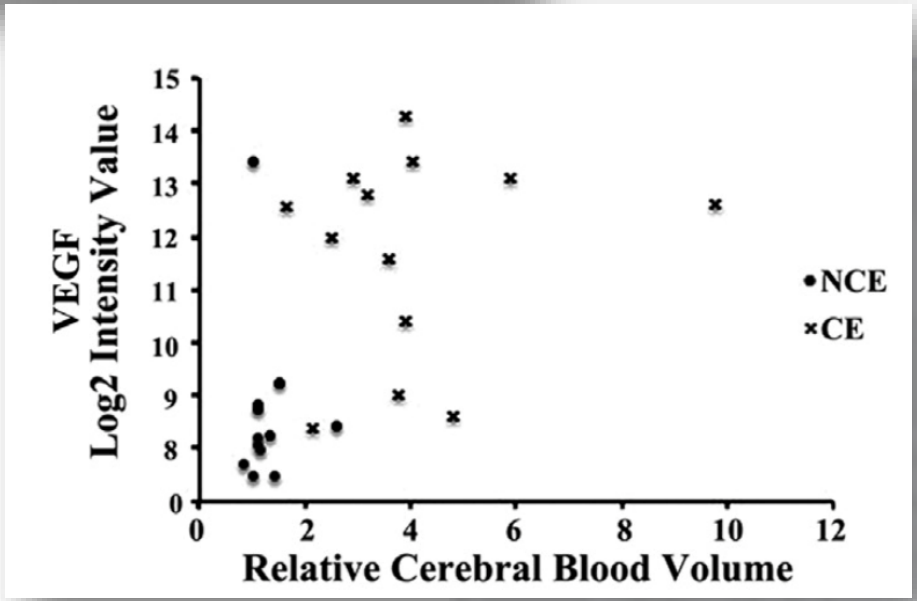

FARMACI ANTI-ANGIOGENETICI

HUMANIZED ANTIVASCULAR ENDOTHELIAL GROWTH FACTOR (anti-VEGF) MONOCLONAL ANTIBODY **BEVACIZUMAB**

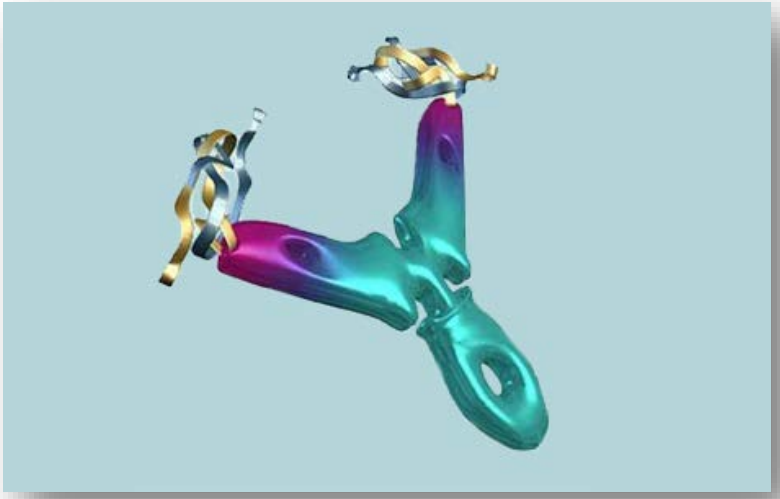

Angiogenesi: benchè sia un processo fisiologico naturale, è richiesto da un tumore per crescere.

GLIOBLASTOMA: uno dei tumori più riccamente vascolarizzati.

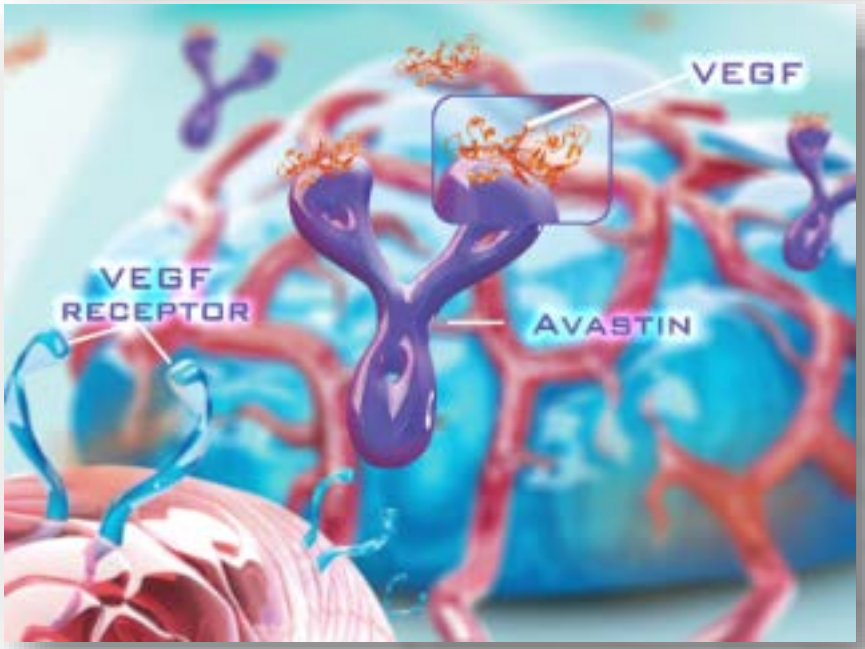

VEGF: importante regolatore dell'angiogenesi, particolarmente presente ed espresso nei tumori cerebrali.
Alti livelli di VEGF si osservano nelle aree di necrosi e nelle regioni con proliferazione endoteliale.
La densità vascolare e l'espressione del VEGF correlano con la malignità e l'aggressività della neoplasia

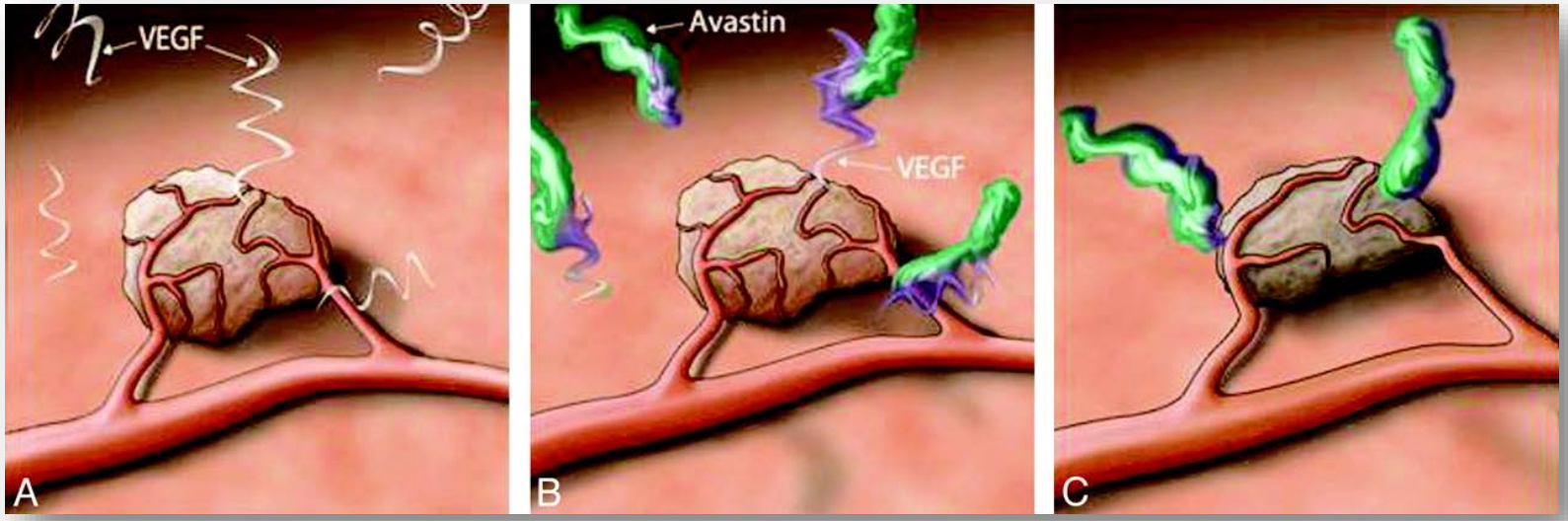

MECCANISMI D'AZIONE:

1. Inibizione diretta dell'angiogenesi tumorale
2. Effetto antigliale sulle cellule che esprimono il recettore VEGF
3. Distruzione delle cellule staminali microvascolari
4. Normalizzazione della funzione vascolare

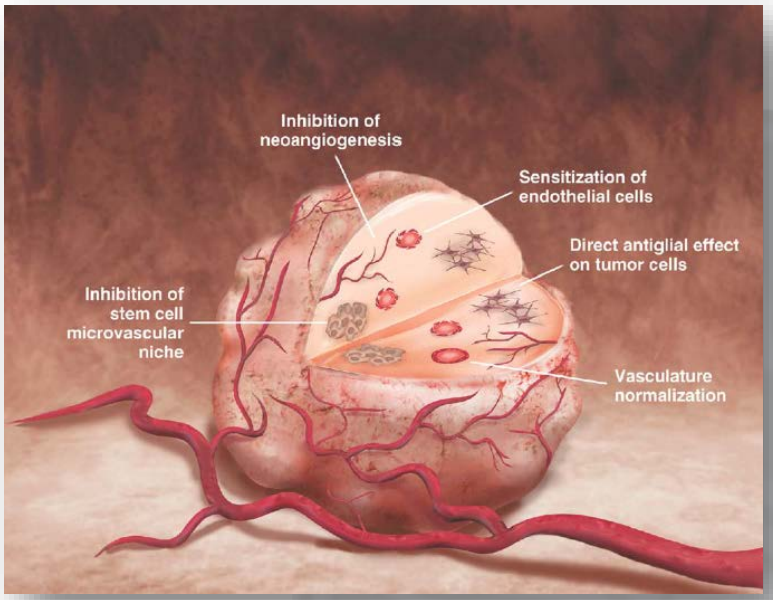

FARMACI ANTI-ANGIOGENETICI

1. BEVACIZUMAB: anticorpo anti-VEGF (vascular endothelial growth factor)
2. CEDIRANIB: tyrosin-kinasi inibitore del recettore VEGF

Rapida diminuzione del potenziamento patologico dopo mdc

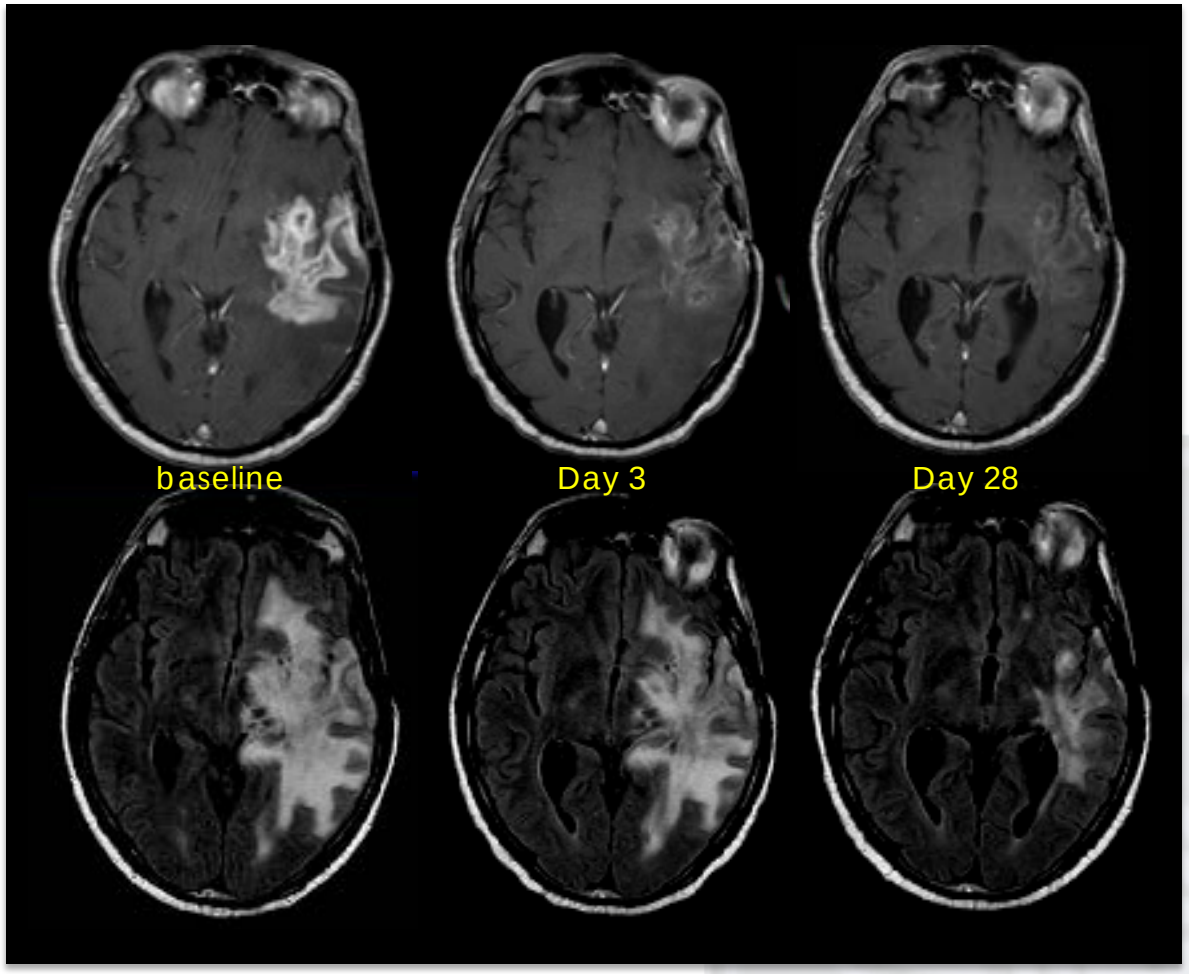

Vera risposta al trattamento

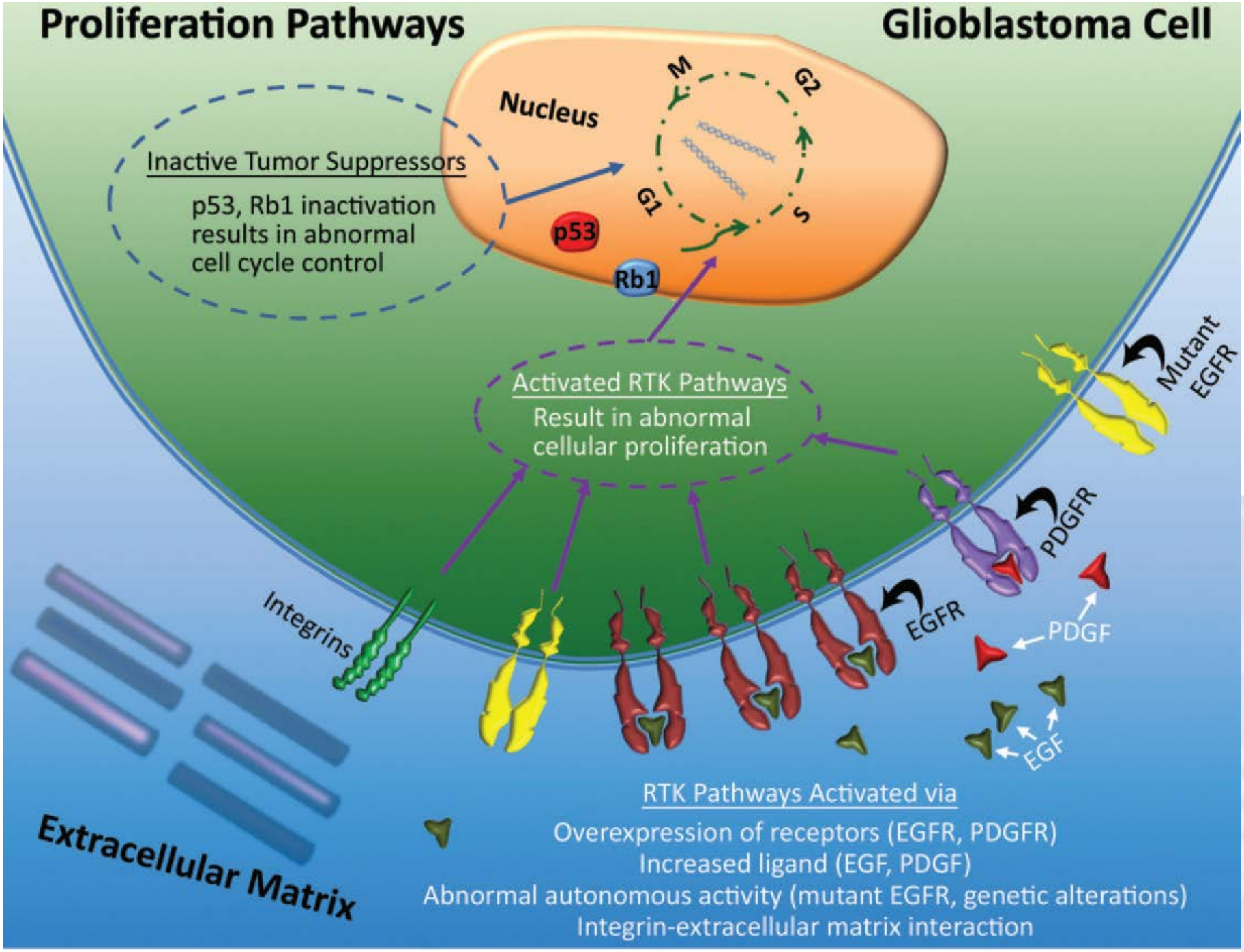
Proliferation Pathways
Glioblastoma Cell
Nucleus
M
G2
G1
S
Inactive Tumor Suppressors
p53, Rb1 inactivation results in abnormal cell cycle control
p53
Rb1
Activated RTK Pathways
Result in abnormal cellular proliferation
Mutant EGFR
PDGFR
EGFR
PDGF
EGF
Integrins
Extracellular Matrix
RTK Pathways Activated via
Overexpression of receptors (EGFR, PDGFR)
Increased ligand (EGF, PDGF)
Abnormal autonomous activity (mutant EGFR, genetic alterations)
Integrin-extracellular matrix interaction

Potential Role of Preoperative Conventional MRI Including Diffusion Measurements in Assessing Epidermal Growth Factor Receptor Gene Amplification Status in Patients with Glioblastoma

R.J. Young, A. Gupta, A.D. Shah, J.J. Graber, A.D. Schweitzer, A. Prager, W. Shi, Z. Zhang, J. Huse, and A.M.P. Omuro

Table 3: Quantitative analysis of ADC correlation with EGFR (n=142)

	EGFR Status*			
	Not Amplified (n=82)	Amplified (n=60)	*P* Value	AUC
ADC_{mean}	1.27 (0.90–1.97)	1.15 (0.11–1.70)	.0007	0.667
ADC_{min}	0.90 (0.16–8.38)	0.83 (0.51–1.23)	.01	0.624
ADC_{max}	2.11 (1.22–3.28)	1.77 (0.86–3.01)	.005	0.639
ADC_{ROI}	1.06 (0.56–1.59)	0.93 (0.67–1.30)	.0003	0.680
ADC_{ratio}	1.37 (0.13–2.33)	1.22 (0.77–1.95)	.003	0.645

Note:—AUC indicates area under the curve.

* Reported as median (range) $\times 10^{-3}$ mm^2/s with *P* values by the Wilcoxon rank sum test.

T1-Weighted Dynamic Contrast-Enhanced MRI as a Noninvasive Biomarker of Epidermal Growth Factor Receptor vIII Status

J. Arevalo-Perez, A.A. Thomas, T. Kaley, J. Lyo, K.K. Peck, A.I. Holodny, I.K. Mellinghoff, W. Shi, Z. Zhang, and R.J. Young

Increased relative plasma volume and increased relative contrast transfer coefficient parameters were both significantly associated with positive epidermal growth factor receptor variant III status.

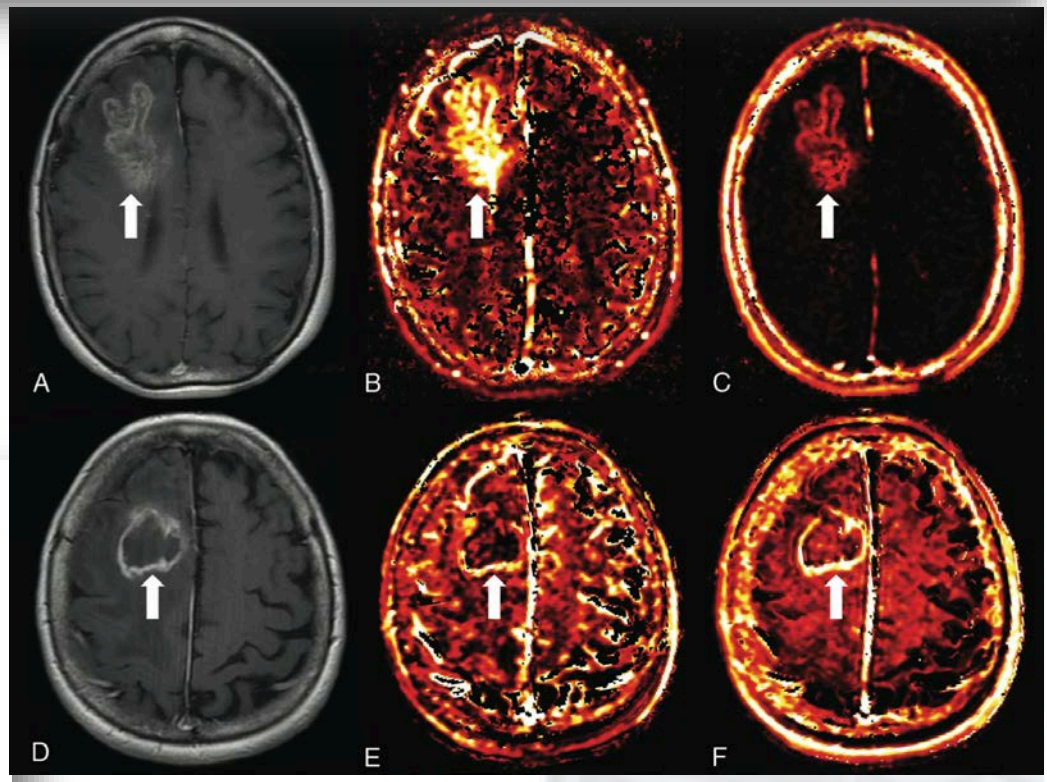

Analysis of the relationship between baseline perfusion parameters and EGFRvIII mutation status

Perfusion Parameter[a]	EGFRvIII Status (Median, Range) Negative (n = 58)	Positive (n = 24)	P Value	AUC
rVP_{mean}	3.6 (1.5–18.1)	9.3 (2.9–29.3)	<.001	0.818
$rVP_{90\%tile}$	5.1 (1.6–19.1)	10.7 (4.1–30.2)	<.001	0.833
$rVP_{75\%tile}$	4.2 (1.6–18.4)	9.2 (3.5–28.1)	<.001	0.821
rK^{trans}_{mean}	3.7 (1.1–20.3)	6.5 (1.7–22.4)	.008	0.688
$rK^{trans}_{90\%tile}$	4.8 (1.5–22.6)	7.6 (2.1–31.8)	.02	0.669
$rK^{trans}_{75\%tile}$	4.2 (1.4–19.7)	6.8 (1.9–24.7)	.007	0.692

Note:—AUC indicates area under the curve in the ROC analysis.

[a] All values are relative ratios normalized to tumor/contralateral normal tissue.

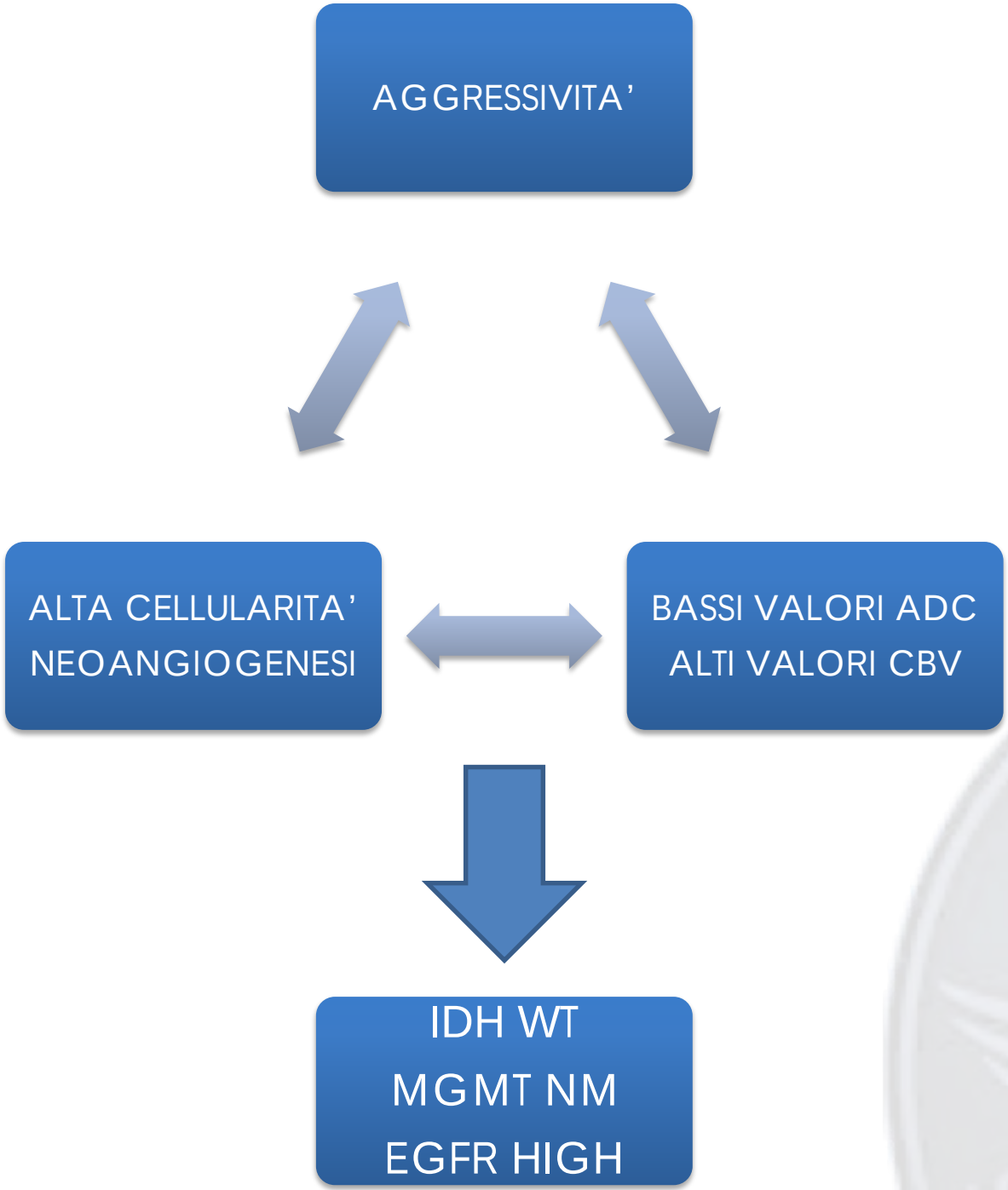
AGGRESSIVITA'
ALTA CELLULARITA'
NEOANGIOGENESI
BASSI VALORI ADC
ALTI VALORI CBV
IDH WT
MGMT NM
EGFR HIGH

O^6-methylguanine methyltransferase (MGMT)

Enzima di riparazione del DNA contro agenti alchilanti come anche la TEMOZOLOMIDE.

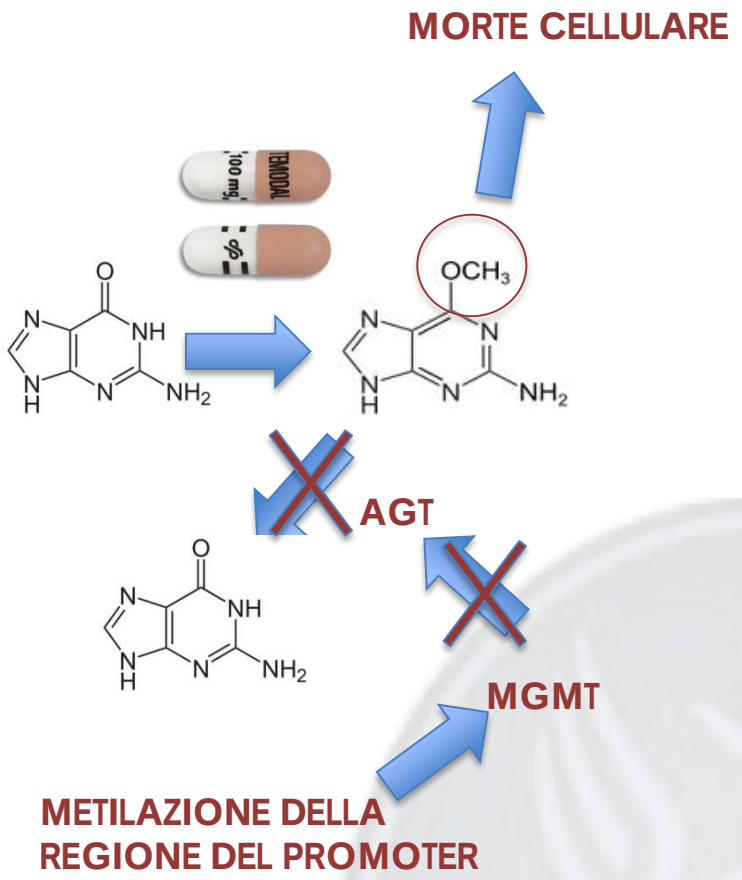

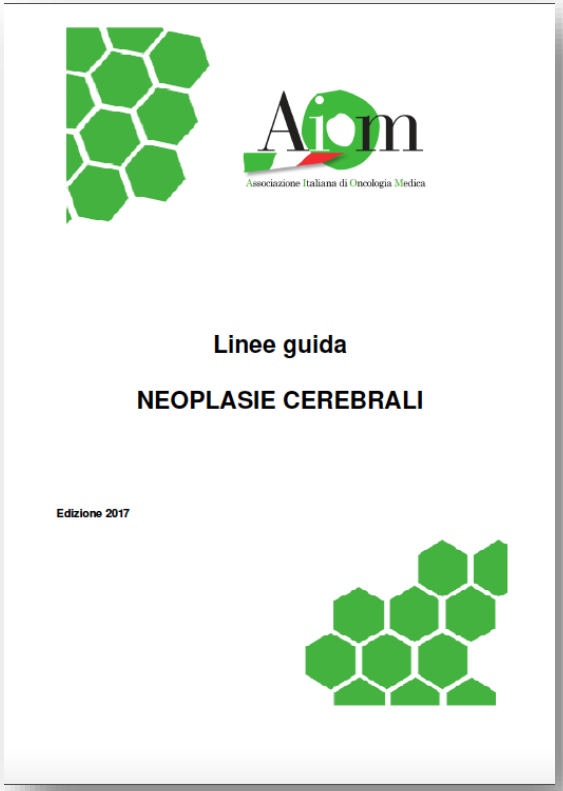

PROTOCOLLO STUPP

CHIRURGIA + RADIOTERAPIA + CHEMIOTERAPIA (TMZ) CONCOMITANTE E ADIUVANTE

L'approccio, valido dal 2005*, migliora i tempi di sopravvivenza (OS & PFS) dei pazienti

*Fase III Trial condotto dalla *European Organization for Research and Treatment of Cancer* (EORTC) e dal *National Cancer Institute of Canada* (NCIC)

FIGURA 1: GBM di nuova diagnosi (1)

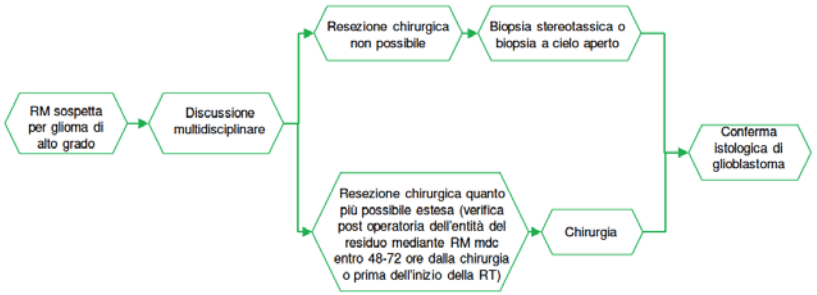

FIGURA 2: GBM di nuova diagnosi (2)

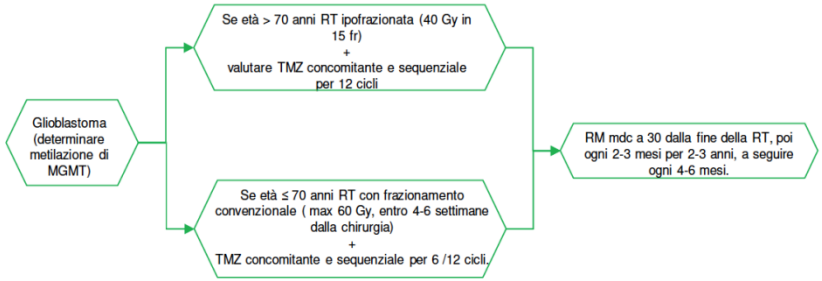

FIGURA 3: Recidiva di glioblastoma

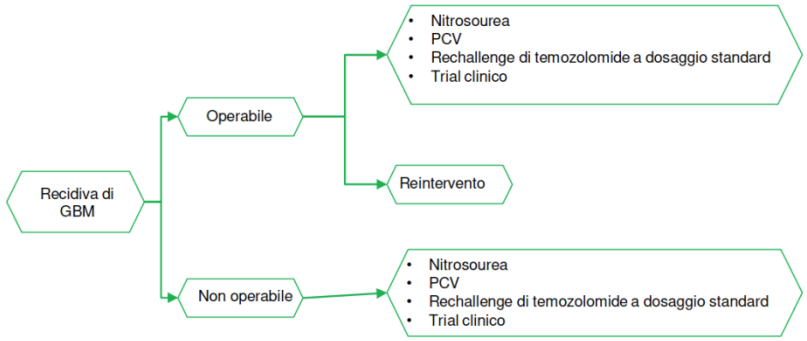

ADC vs MGMT

Eur Radiol
DOI 10.1007/s00330-012-2601-4

NEURO

Apparent diffusion coefficient obtained by magnetic resonance imaging as a prognostic marker in glioblastomas: correlation with MGMT promoter methylation status

Andrea Romano · L. F. Calabria · F. Tavanti · G. Minniti · M. C. Rossi-Espagnet · V. Coppola · S. Pugliese · D. Guida · G. Francione · C. Colonnese · L. M. Fantozzi · A. Bozzao

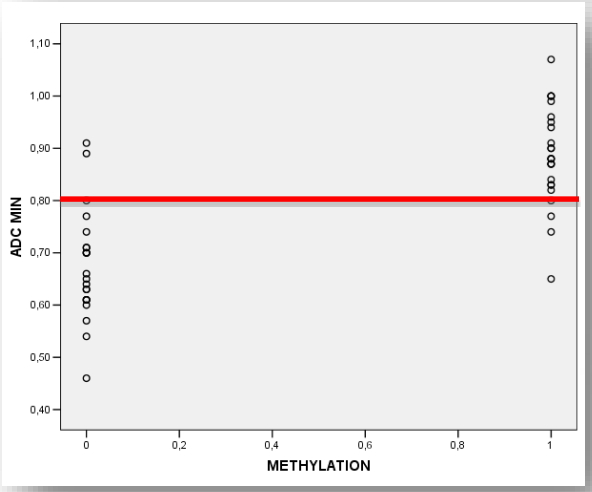

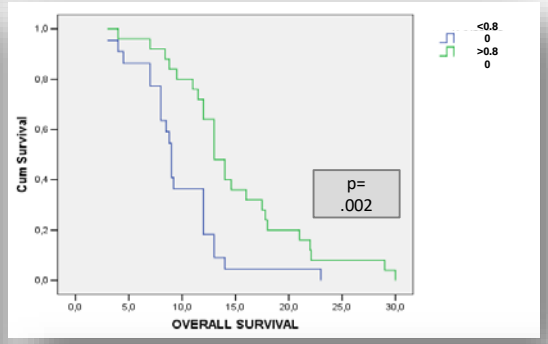

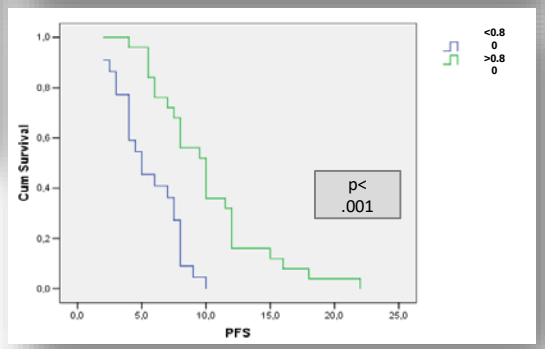

sensibilità (84%)
specificità (91%)

ADC minimo: 0.80x10^{-3}mm^2/sec

1.Pope et al. AJNR 2011 *(52 pz valutati dopo la chirurgia e trattati con Bevacizumab)*

1.Moon et al. Neuroradiology 2012*

1.Romano et al Eur Radiol 2012*

1.Sunwoo et al J Magn Reson Imaging 2012*

1.Gupta et al AJNR 2013

ORIGINAL RESEARCH
ADULT BRAIN

Clinically Relevant Imaging Features for *MGMT* Promoter Methylation in Multiple Glioblastoma Studies: A Systematic Review and Meta-Analysis

C.H. Suh, H.S. Kim, S.C. Jung, C.G. Choi, and S.J. Kim

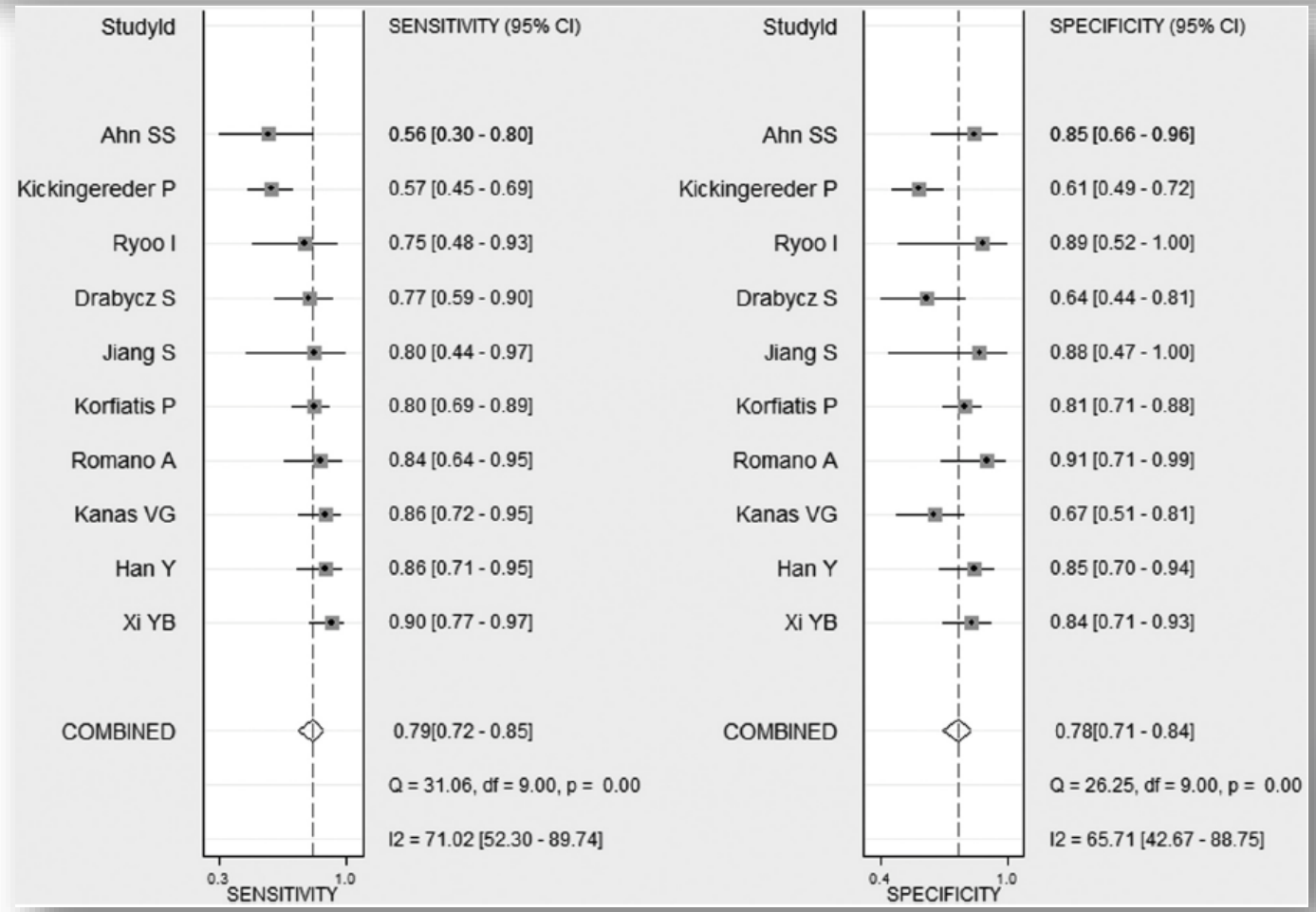

22 articles including 2199 patients.
MGMT promoter methylated glioblastoma:
-less edema,
-high ADC,
-low perfusion.

Structural and advanced imaging in predicting MGMT promoter methylation of primary glioblastoma: a region of interest based analysis

Yu Han[1†], Lin-Feng Yan[1†], Xi-Bin Wang[2], Ying-Zhi Sun[1], Xin Zhang[1], Zhi-Cheng Liu[1], Hai-Yan Nan[1], Yu-Chuan Hu[1], Yang Yang[1], Jin Zhang[1], Ying Yu[1], Qian Sun[1], Qiang Tian[1], Bo Hu[1], Gang Xiao[1], Wen Wang[1*] and Guang-Bin Cui[1*]

Table 3

Differences in ADC and rCBF values between MGMT (−) and MGMT (+) ($\bar{x}\pm s$)

Values	MGMT(−)	MGMT(+)	t	*P*-value*
rCBF	9.467 ± 2.706	5.916 ± 2.518	5.945	< 0.001
ADC ($\times10^{-3}$ mm^2/s)	0.729 ± 0.085	0.899 ± 0.137	6.514	< 0.001

DWI and and 3-dimensional pseudo-continuous arterial spin labeling (3D pCASL) imaging.

Table 4

ROC and LOOCV of ADC and rCBF values for differentiating MGMT (

Values	AUC	Sensitivity (%)	Specificity (%)	Cutoff value
rCBF	0.835	75.0	78.4	7.680
ADC ($\times10^{-3}$ mm^2/s)	0.860	81.1	82.5	0.792

Table 5 Comparison of AUC of the varied MRI parameter combinations

Values	AUC	Sensitivity (%)	Specificity (%)	LOOCV Accuracy (%)	LOOCV AUC
rCBF + ADC	0.893	83.1	83.2	81.8	0.871
Location + Necrosis	0.670	62.3	62.3	53.2	0.597
rCBF + Location + Necrosis	0.852	77.9	77.6	72.7	0.821
ADC + Location + Necrosis	0.891	80.5	80.2	79.2	0.845
ALL	0.914	85.7	85.2	80.5	0.877

Note: ADC = apparent diffusion coefficient, rCBF = relative cerebral blood flow, AUC = area under ROC curve, LOOCV = leave-one-out cross-validation, ALL = ADC + rCBF + Location + Necrosis

ORIGINAL RESEARCH
BRAIN

Probabilistic Radiographic Atlas of Glioblastoma Phenotypes

B.M. Ellingson, A. Lai, R.J. Harris, J.M. Selfridge, W.H. Yong, K. Das, W.B. Pope, P.L. Nghiemphu, H.V. Vinters, L.M. Liau, P.S. Mischel, and T.F. Cloughesy

507 pazienti

433 pazienti – 38% MGMT+
400 pazienti – 8,5% IDH1 mutato

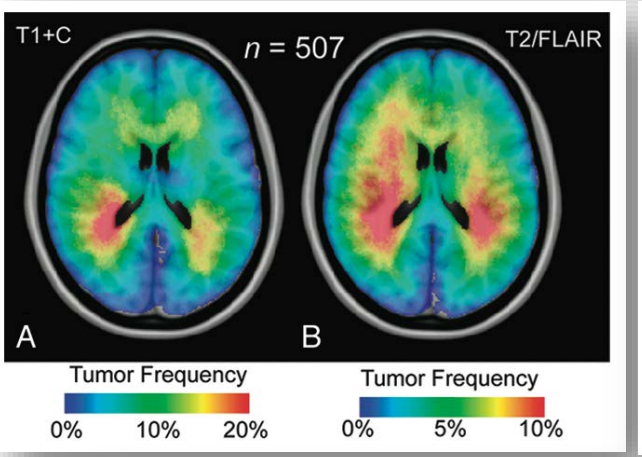

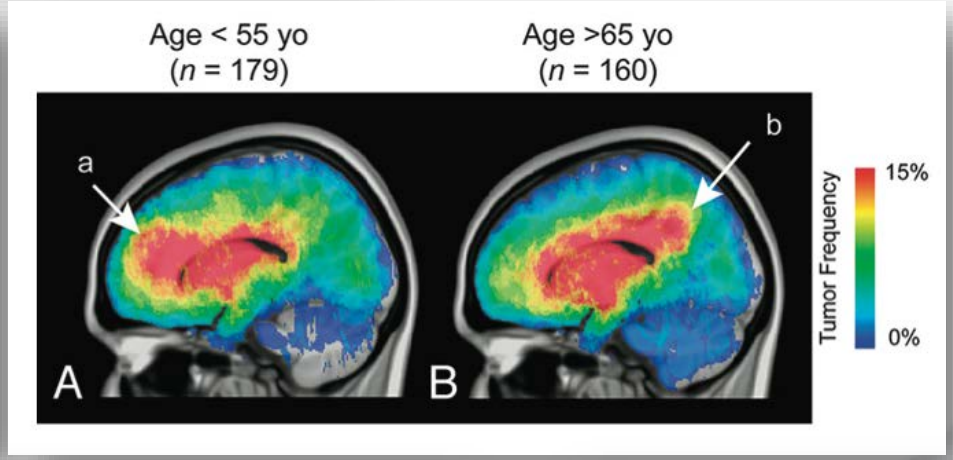

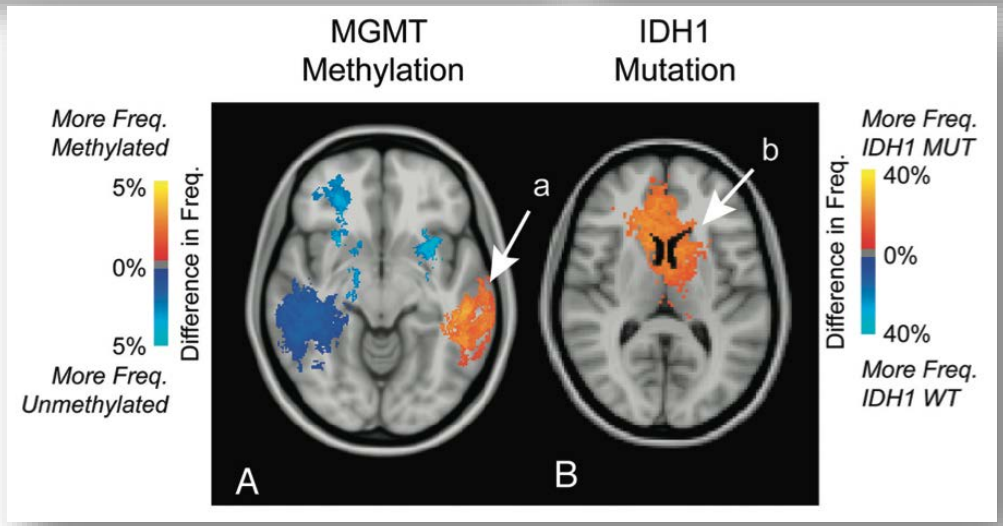

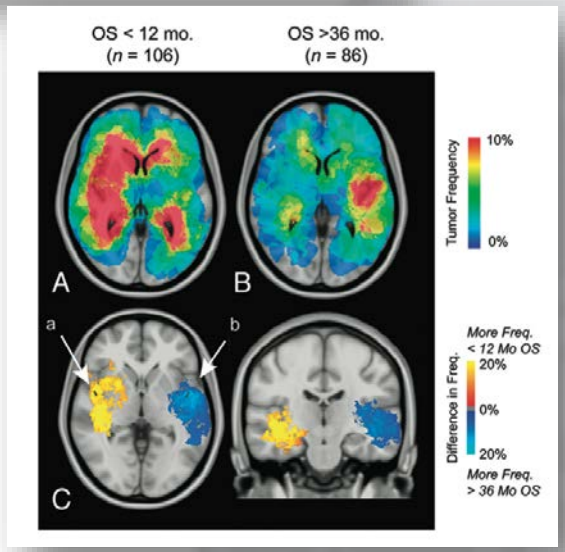

‘QUESTIONI’ APERTE

1536 Neuro-Oncology
20(11), 1536–1546, 2018 | doi:10.1093/neuonc/noy066 | Advance Access date 28 April 2018

Intratumoral heterogeneity of oxygen metabolism and neovascularization uncovers 2 survival-relevant subgroups of IDH1 wild-type glioblastoma

Andreas Stadlbauer, Max Zimmermann, Arnd Doerfler, Stefan Oberndorfer, Michael Buchfelder, Roland Coras, Melitta Kitzwögerer, and Karl Roessler

- **Quantitative BOLD approach** (multi-echo GE sequence for R2* mapping and multi-echo SE sequence for R2-mapping) and **DSC perfusion** biomarkers
  ⇨ fused in a single map of **tumor microenvironment (TME)**
- **TME map** ⇨ heterogeneity, spatial localization, and extent of **necrosis**, **hypoxia**, **OxPhos**, and **glycolysis** combined with/without neovascularization

Glycolytic phenotype with stable neovasculature

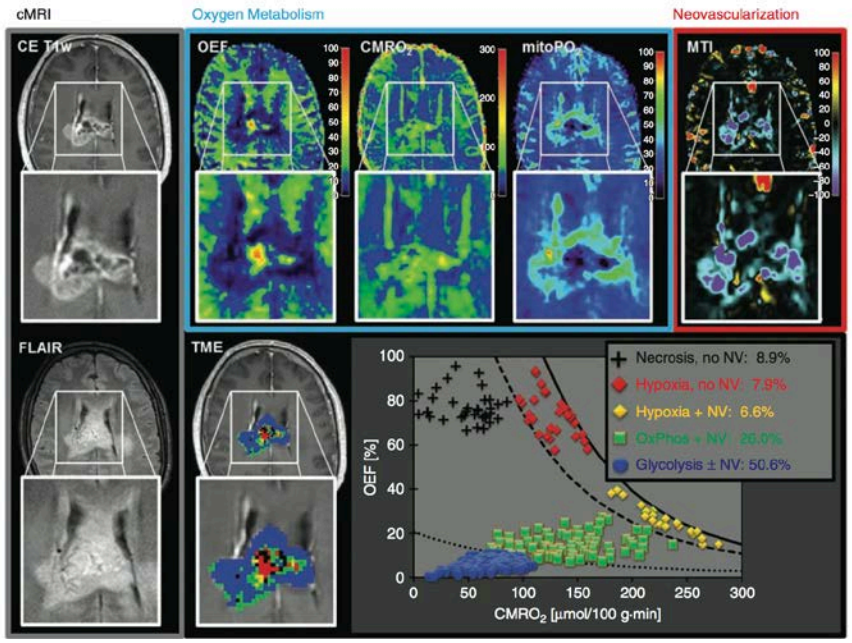

Necrotic/hypoxic phenotype with disfunctional NV

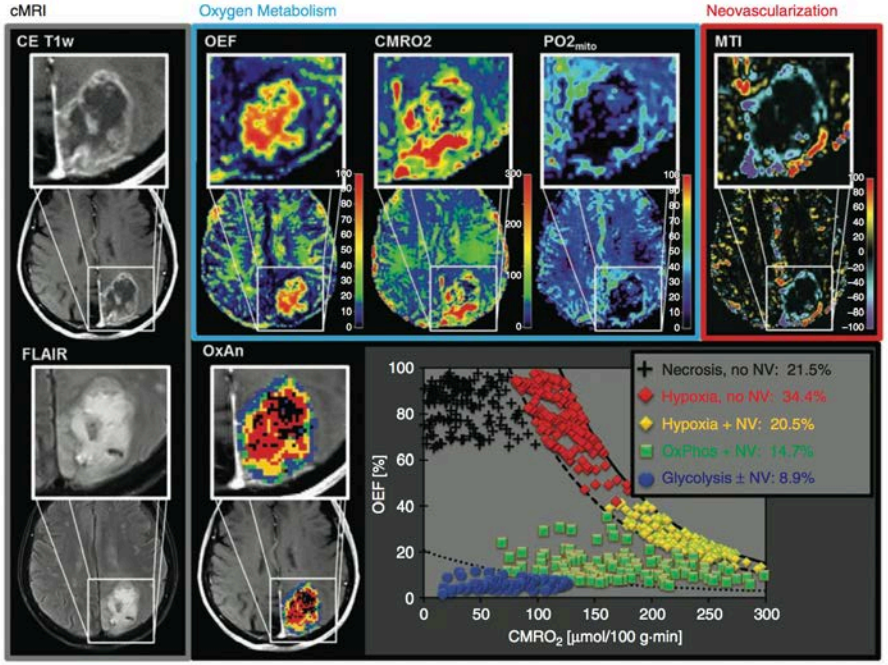

Mapping intratumoral heterogeneity of GBM metabolism

1536 Neuro-Oncology
20(11), 1536–1546, 2018 | doi:10.1093/neuonc/noy066 | Advance Access date 28 April 2018

Intratumoral heterogeneity of oxygen metabolism and neovascularization uncovers 2 survival-relevant subgroups of IDH1 wild-type glioblastoma

Andreas Stadlbauer, Max Zimmermann, Arnd Doerfler, Stefan Oberndorfer, Michael Buchfelder, Roland Coras, Melitta Kitzwögerer, and Karl Roessler

- Glycolytic phenotype with stable functional neovasculature ⇨ longer PFS
- Necrotic/hypoxic phenotype with high proportion of unstable, defective dysfunctional neovasculature ⇨ more aggressive tumor behavior
- **Possible detection of hypoxic and vascular niches in GBMs**

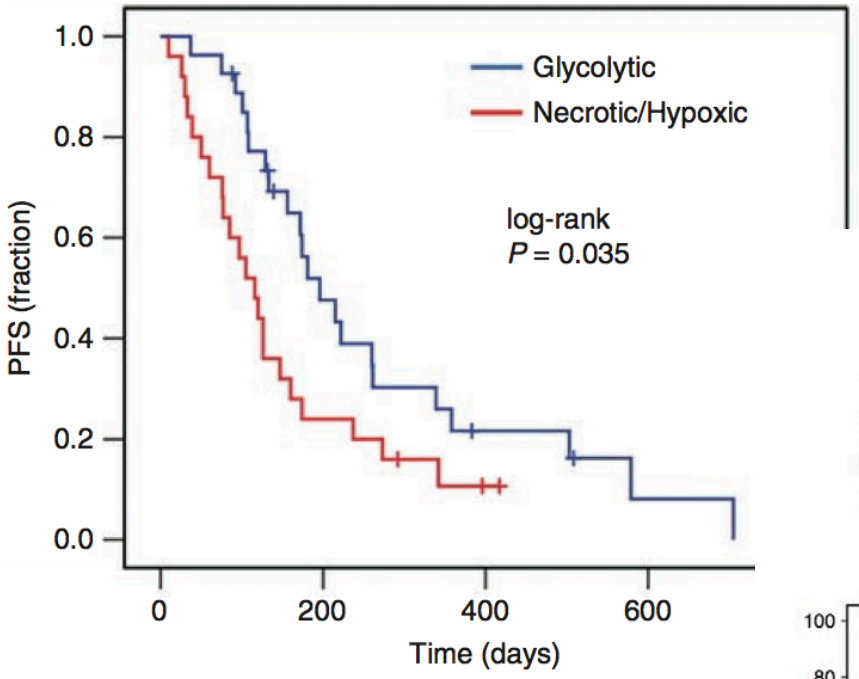

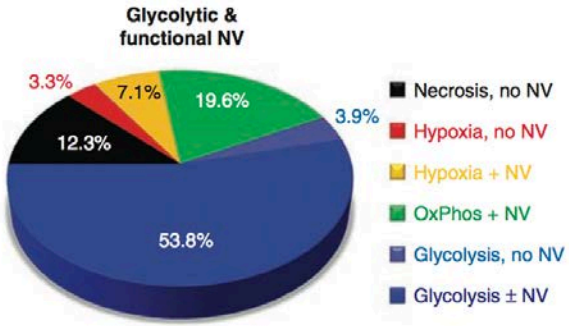

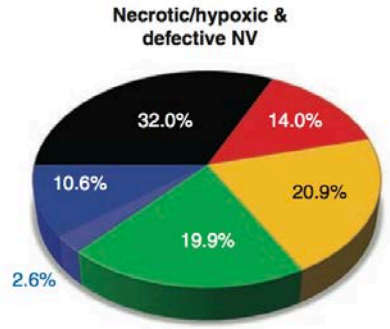

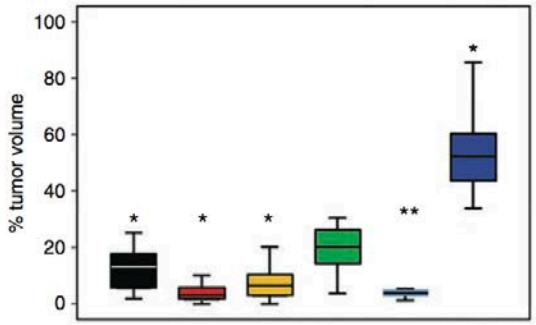

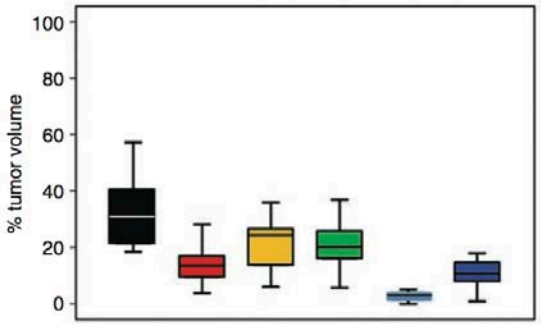

RADIOMICA E RADIOGENOMICA

- RADIOMICA _ estrazione di dati **quantitativi** dalle immagini di RM convenzionale e di tecniche avanzate
- RADIOGENOMICA_associazione tra biomarcatori radiomici, firme genomiche e fenotipi molecolari

Smits M and Van Den Bent MJ, Radiology 284, 316-331 (2017)
Abrol, S. et al. Top Magn Reson Imaging 26, 43-53 (2017)

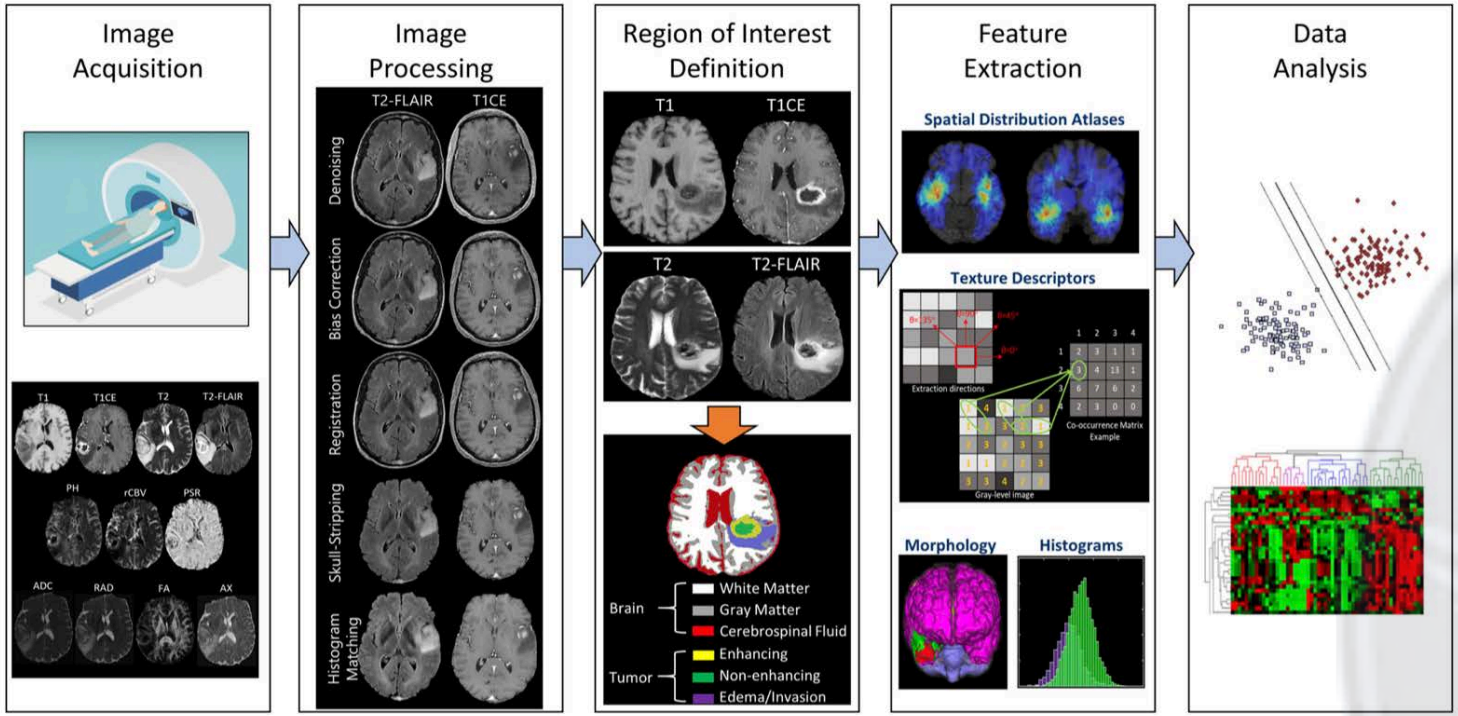

Published online 2019 Oct 8. doi: 10.1038/s41598-019-50849-y PMID: 31594994

Radiomics and *MGMT* promoter methylation for prognostication of newly diagnosed glioblastoma

Takahiro Sasaki,[1,2,3] Manabu Kinoshita,[2,4,5] Koji Fujita,[2,3] Junya Fukai,[2,3] Nobuhide Hayashi,[1,2] Yuji Uematsu,[2,3] Yoshiko Okita,[2,6] Masahiro Nonaka,[2,6,7] Shusuke Moriuchi,[2,6,8] Takehiro Uda,[2,9] Naohiro Tsuyuguchi,[2,9,10] Hideyuki Arita,[2,5] Kanji Mori,[2,11] Kenichi Ishibashi,[2,12] Koji Takano,[2,13] Namiko Nishida,[2,14] Tomoko Shofuda,[2,15] Ema Yoshioka,[2,15] Daisuke Kanematsu,[2,16] Yoshinori Kodama,[2,17] Masayuki Mano,[2,18] Naoyuki Nakao,[2,3] and Yonehiro Kanemura[2,6,19]

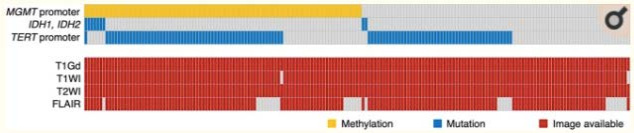

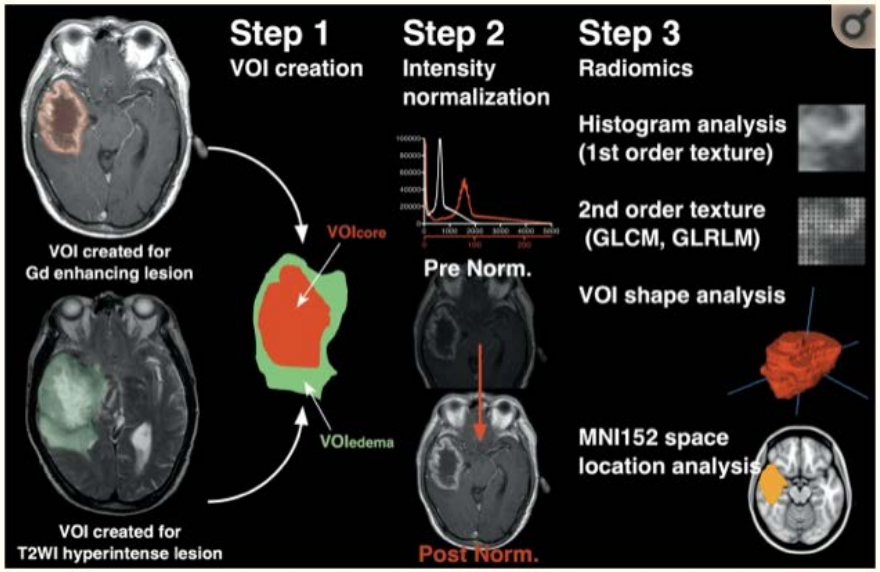

Figure 2

Illustration showing the workflow for image analysis. Two types of VOIs were created based on Gd enhancement of the tumor and edema lesion identification on T2-weighted images. Both VOIs were co-registered, and VOI_{core} and VOI_{edema} were generated. Subsequently, intensity normalization of all images was performed, and first-order and second-order texture analysis, VOI shape analysis, and location analysis were performed.

Prediction accuracy of *pMGMT* methylation status with radiomics.

	Average of 5 repetitive measures
Accuracy	67%
Sensitivity	67%
Specificity	66%
Positive predictive value	67%
Negative predictive value	67%
Prevalence of *pMGMT* methylation	50%

Conclusion

Go to:

The current study revealed that radiomics can be used to build a prognostic score stratifying high- and low-risk GBM; this score was an independent prognostic factor from *pMGMT* methylation status. On the other hand, predictive accuracy of *pMGMT* methylation status by radiomic analysis was 67%, which remains insufficient for practical use. A combination of radiomic score and *pMGMT* methylation status effectively provided a more accurate stratification of clinical outcomes for newly diagnosed GBM patients.

Percorso Didattico Scientifico Specializzazione Radio-Oncologia

GRAZIE DELL'ATTENZIONE

Giulia Butera

31-01-2020